UNIVERSITY OF CALIFORNIA SAN DIEGO

Liposome Encapsulation to Enhance Adenovirus Stealth and Transduction Efficiency in Invasive Breast Cancer

A Dissertation submitted in partial satisfaction of the requirements
for the degree of Doctor of Philosophy

in

Nanoengineering

by

Abraham Tac Phung

Committee in charge:

Professor Andrew C. Kummel, Chair
Professor Jesse Jokerst, Co-Chair
Professor Sarah Blair
Professor Willliam Trogler
Professor Liangfang Zhang

2025

The Dissertation of Abraham Tac Phung is approved, and it is acceptable in quality and form for publication on microfilm and electronically.

University of California San Diego

2025

DEDICATION

This work is dedicated to my friends and family for all their love and support.

TABLE OF CONTENTS

LIST OF FIGURES

LIST OF TABLES

ACKNOWLEDGEMENTS

This milestone would not be possible without the support and guidance of my advisor, Professor Andrew Kummel. He taught me the importance of persistence and a consistent work ethic in the pursuit of scientific progress. I would also like to thank the Reid lab, Professor William Trogler, Professor Sarah Blair, and Professor Omonigho Aisagbonhi for their overwhelming support and insight. The immense wealth of knowledge exchanged throughout our collaborations and discussions helped me countlessly throughout my graduate experience.

My achievements would also not be possible without my lab mates Dr. Jaimin Shah and Dr. Tao Dong. I want to thank them both for being such supportive teammates and friends to me throughout my graduate career. Their continuous enthusiasm and encouragement helped build and maintain the warm, cooperative work environment each day in the lab.

I would like to also thank my committee members, Professor Andrew Kummel, Professor William Trogler, Professor Jesse Jokerst, Professor Liangfang Zhang, and Professor Sarah Blair for the opportunity to defend my dissertation before them. Without their help and feedback, I would not have been able put together this comprehensive archive of my graduate work at UC San Diego.

Finally, I want to give thanks to my family and friends all their love and support. I would like to thank my mother, Kathy Phung, for all her love and care, and for always cheering me on in endeavors. I would like to thank my sister, Dr. Elizabeth Phung-Hart, for always encouraging me to work hard and reminding me to take care of myself. I want to thank my brother, Christopher Phung, for always watching out for me and being willing to help at any moment. I want to thank my brother, Dr. Theodore Phung, for always fueling my academic curiosities and

being my emotional support. I finally want to thank my sister, Isabella Phung, for being a constant inspiration for me to do the things I love.

Chapter 1, in full, is a reprint of the material as it appears in Breast Cancer Research 2024. Phung, Abraham T.; Shah, Jaimin R.; Dong, Tao; Reid, Tony; Larson, Christopher; Sanchez, Ana B.; Oronsky, Bryan; Trogler, William C.; Kummel, Andrew C.; Aisagbonhi, Omonigho; Blair, Sarah L. Springer Nature, 2024. The dissertation author was the primary author of this paper.

Chapter 2, in full, is a reprint of the material as it appears in Pharmaceutics 2025. Phung, Abraham T.; Shah, Jaimin R.; Dong, Tao; Aisagbonhi, Omonigho; Trogler, William C.; Kummel, Andrew C.; Blair, Sarah L. MDPI, 2025. The dissertation author was the primary author of this paper.

VITA

2015 Bachelor of Science in Biomedical Engineering, University of California, Irvine

2019 Master of Science in Nanoengineering, University of California San Diego

2025 Doctor of Philosophy in Nanoengineering, University of California San Diego

PUBLICATIONS

Phung AT, Shah JR, Dong T, Aisagbonhi O, Trogler WC, Kummel AC, Blair SL. Adenoviruses Encapsulated in PEGylated DOTAP-Folate Liposomes Are Protected from the Pre-Existing Humoral Immune Response. Pharmaceutics. 2025 Jun 11;17(6):769.

Phung AT, Shah JR, Dong T, Reid T, Larson C, Sanchez AB, Oronsky B, Trogler WC, Kummel AC, Aisagbonhi O, Blair SL. CAR expression in invasive breast carcinoma and its effect on adenovirus transduction efficiency. Breast Cancer Research. 2024 Sep 10;26(1):131.

Dong T, Shah JR, Phung AT, Blair SL, Trogler WC, Kummel AC, Hayashi T. Liposomal Oncolytic Adenovirus Enables Efficient CAR-independent Transduction of Tumors and Enhances NK Cell-mediated Abscopal Responses. ACS Applied Materials & Interfaces. (Submitted 2025 Aug 07)

Shah JR, Dong T, Phung AT, Khan S, Aisagbonhi O, Blair SL, Bouvet M, Trogler WC, Kummel AC. Liposomal oncolytic adenovirus as a neoadjuvant therapy for triple-negative breast cancer. Scientific Reports. 2025 May 14;15(1):16737.

Dong T, Shah JR, Phung AT, Larson C, Sanchez AB, Aisagbonhi O, Blair SL, Oronsky B, Trogler WC, Reid T, Kummel AC. A local and abscopal effect observed with liposomal encapsulation of intratumorally injected oncolytic adenoviral therapy. Cancers. 2023 Jun 12;15(12):3157.

Shah JR, Dong T, Phung AT, Reid T, Larson C, Sanchez AB, Oronsky B, Blair SL, Aisagbonhi O, Trogler WC, Kummel AC. Development of Adenovirus containing liposomes produced by Extrusion vs. homogenization: a comparison for Scale-Up purposes. Bioengineering. 2022 Oct 27;9(11):620.

Huang CH, Dong T, Phung AT, Shah JR, Larson C, Sanchez AB, Blair SL, Oronsky B, Trogler WC, Reid T, Kummel AC. Full remission of CAR-deficient tumors by DOTAP-folate liposome encapsulation of adenovirus. ACS Biomaterials Science & Engineering. 2022 Nov 17;8(12):5199-209.

FIELD OF STUDY

Major Field: Nanoengineering
Studies in Cancer Nanobiotechnology
Professor Andrew C. Kummel

ABSTRACT OF THE DISSERTATION

Liposome Encapsulation to Enhance Adenovirus Stealth and Transduction Efficiency in Invasive Breast Cancer

by

Abraham Tac Phung

Doctor of Philosophy in Nanoengineering

University of California San Diego, 2025

Professor Andrew C. Kummel, Chair

Professor Jesse Jokerst, Co-Chair

Invasive breast cancer is one of the leading causes of death in women, where patients with invasive lobular carcinoma (ILC) face poor long-term clinical outcomes due to challenges in detection and treatment. Systemic oncolytic adenoviral therapy has shown promise as a novel therapeutic option; however, it is limited by the coxsackievirus & adenovirus receptor (CAR)

expression by the tumor cells and neutralization of the adenovirus by antibodies in the blood. To overcome these limitations, a PEGylated-liposome coating was developed to encapsulate adenoviruses. CAR expression data combined with transduction experiments revealed that ILC demonstrates low CAR expression and liposome-encapsulated adenovirus (DfAd) improved adenoviral transduction in ILC cells by 4-fold by bypassing CAR-dependent transfection mechanisms. To evaluate the protective capabilities of the liposome from neutralizing neutralizing antibodies, a novel in vivo assay using immunized mouse models revealed that DfAd improved protection from neutralizing antibodies in the blood by at least 12-fold. In vitro optimization of DfAd revealed PEG as a critical component for both liposome stability and protection against neutralizing antibodies. This work demonstrates liposome-encapsulation as a promising solution for improving systemic oncolytic adenoviral therapy for breast cancer patients and provides insights for clinical translation of systemic oncolytic viral therapies.

Chapter 1 CAR Expression in Invasive Breast Carcinoma and its Effect on Adenovirus Transduction Efficiency

1.1 Abstract

Breast cancer is the second leading cause of death in women, with invasive ductal carcinoma (IDC) and invasive lobular carcinoma (ILC) as the two most common forms of invasive breast cancer. While estrogen receptor positive (ER+) IDC and ILC are treated similarly, the multifocality of ILC presents challenges in detection and treatment, worsening long-term clinical outcomes in patients. With increasing documentation of chemoresistance in ILC, additional treatment options are needed. Oncolytic adenoviral therapy may be a promising option, but cancer cells must express the coxsackievirus & adenovirus receptor (CAR) for adenoviral therapy to be effective. The present study aims to evaluate the extent to which CAR expression is observed in ILC in comparison to IDC, and how the levels of CAR expression correlate with adenovirus transduction efficiency. The effect of liposome encapsulation on transduction efficiency is also assessed. To characterize CAR expression in invasive breast carcinoma, 36 formalin-fixed paraffin-embedded (FFPE) human breast tumor samples were assayed by CAR immunohistochemistry (IHC). Localization of CAR in comparison to other junctional proteins was performed using a multiplex immunofluorescence panel consisting of CAR, p120-catenin, and E-cadherin. ILC and IDC primary tumors and cell lines were transduced with E1- and E3-deleted adenovirus type 5 inserted with a GFP transgene (Ad-GFP) and DOTAP liposome encapsulated Ad-GFP (DfAd-GFP) at various multiplicities of infection (MOIs). Transduction efficiency was measured using a fluorescence plate reader. CAR expression in the human primary breast carcinomas and cell lines was also evaluated by IHC. We observed

membranous CAR, p120-catenin and E-cadherin expression in IDC. In ILC, we observed cytoplasmic expression of CAR and p120-catenin, with absent E-cadherin. Adenovirus effectively transduced high- CAR IDC cell lines, at MOIs as low as 12.5. Ad-GFP showed similar transduction as DfAd-GFP in high-CAR IDC cell lines. Conversely, Ad-GFP transduction of ILC cell lines was observed only at MOIs of 50 and 100. Furthermore, Ad-GFP did not transduce CAR-negative IDC cell lines even at MOIs greater than 100. Liposome encapsulation (DfAd-GFP) improved transduction efficiency 4-fold in ILC and 17-fold in CAR-negative IDC cell lines.

1.2 Introduction

Invasive ductal carcinoma (IDC) and invasive lobular carcinoma (ILC) are the two most commonly occurring types of invasive breast cancer. IDC makes up 70–80% of breast cancer cases while ILC makes up only about 8–15% of breast cancer cases [1]. Compared to IDC, ILC is more difficult to detect by mammography due to its diffuse growth pattern, slow proliferation, and ill-defined margins [2, 3]. Therefore, ILC presents more frequently in older patients with larger tumors, later stage disease, and more nodal involvement [4,5,6,7], leading to poorer long-term outcomes [1, 4,5,6,7,8]. Patients with ILC are also at higher risk of late recurrences and bone metastasis, than those with similar grade and stage IDC [2, 9].

Oncolytic viral therapy is an emerging treatment option for a variety of cancers, including breast cancers [10]. Currently, adenoviruses remain one of the safest, most efficient and robust viral platforms to engineer gene therapy vectors and oncolytic viruses [11, 12]. In the last decade, several experimental oncolytic adenoviruses have been developed to treat breast [13, 14], gastrointestinal [15, 16], ovarian [17, 18], and brain cancers [19, 20]. Some oncolytic adenoviruses have completed Phase I clinical trials, including AdAPT-001, OBP-301, VCN-01,

and ICOVIR-5 [21,22,23,24]. Oncolytic adenoviral therapy relies on receptor-based transduction through the coxsackievirus & adenovirus receptor (CAR) for most serotypes to infect, replicate inside of, and lyse cancer cells [11, 12, 25, 26]. Therefore, CAR expression in tumors affects adenoviral transduction efficiency.

Liposome encapsulation of oncolytic adenoviruses enables the virus to enter and transduce cancer cells without CAR expression on the surface of their membranes [27,28,29,30]. When the adenovirus is encapsulated in a liposome, the virus can enter the cell through membrane fusion, thereby bypassing the need for CAR-mediated entry [28,29,30]. Other serotype adenoviruses, such as Ad3, and chimeric adenoviruses, such as Ad5F35, can also bypass CAR-mediated entry; however, their transduction efficiency is still limited by the expression of other receptors, such as CD46 in the case of Ad3 and Ad5F35, and require additional fiber protein modifications to overcome these limitations [31]. The advantage of liposome-enhanced delivery of adenoviruses is that the transduction efficiency is independent of fiber receptor expression [32, 33]. Studies in pancreatic, liver, ovarian, and lung cancer models have demonstrated that liposome encapsulation improves the transduction of adenovirus [34,35,36,37].

IDC typically demonstrates moderate to high levels of CAR, and there are some pre-clinical data on the effects of adenoviral therapy on IDC models. However, there are limited studies on CAR expression and the effect of adenoviral therapy in ILC models [38,39,40,41]. The current study aimed to evaluate the extent to which CAR expression is observed in ILC in comparison to IDC and to assess how the levels of CAR expression correlate with adenovirus transduction efficiency. The effect of liposome encapsulation on viral transduction efficiency was also studied using adenovirus encapsulated in DOTAP-folate liposomes (DfAd). While

previous studies demonstrate the promising effects of DfAd in a variety of tumors [27,28,29,30], the effect of heterogenous spatial expression of CAR in IDC and ILC tumors on adenoviral therapy has yet to be investigated. The present study characterized the spatial expression of CAR in a large cohort of patient-derived IDC and ILC samples and evaluated the effects of CAR expression on adenoviral transduction. This study also characterized the expression and localization of the adherens junction proteins, E-cadherin and p120-catenin, in relation to CAR expression in IDC and ILC.

1.3 Materials and methods

1.3.1 Reagents and cell lines

Replication-deficient adenovirus expressing green fluorescent protein (Ad-GFP) was purchased from Baylor College of Medicine (Catalog: Ad5-CMV-eGFP). MCF7 cell line was from the laboratory of Dr. Tony Reid. The SUM44PE cell line was purchased from BioIVT (Catalog: HUMANSUM-0003016). Dulbecco's modified Eagle's medium (DMEM) with high glucose (Hyclone #SH30081.01) was supplemented with 10% fetal bovine serum (FBS, Omega Scientific #FB-01) and 1% Pen Strep Glutamine (PSG, Life Technologies #10378-016) to prepare the complete media for MCF7 cell culturing. Ham's F-12 (Life Technologies #11765054) was supplemented with 1 g/L Bovine Serum Albumin (BSA, Sigma Aldrich #A8806), 5 mM of Ethanolamine (Sigma Aldrich #E0135), 10 mM of HEPES (Sigma Aldrich H3375), 1 µg/mL of Hydrocortisone (Sigma Aldrich #H4001), 5 µg/mL of Insulin (Sigma Aldrich #I9278), 50 nM of Sodium Selenite (Sigma Aldrich #S9133), 5 µg/mL of apo-Transferrin (Sigma Aldrich #T2252), 10 nM of Triiodo Thyronine (T3, Sigma Aldrich #T5516), and 2% FBS to prepare the complete media for the SUM44PE cell line. Rosewell Park Memorial Institute (RPMI) 1640 (Gibco #11875093) medium was supplemented with 10% FBS and 1%

PSG to prepare complete RPMI medium. A 1:1 mix of complete DMEM and complete RPMI medium was prepared to culture the MDA-MB-231 cell line. Human tumor digestion buffer was prepared with DMEM/F12 + GlutaMAX (Gibco #10565018) supplemented with 10 mM HEPES, 2% BSA, 5 µg/mL insulin, 0.5 µg/mL hydrocortisone, and 50 µg/mL gentamycin. Human tumor digestion buffer was also prepared using RPMI 1640 and the human tumor dissociation kit (Miltenyi Biotec #130-095-929).

Primary human breast cell medium was prepared by supplementing DMEM/F12 (1:1) with HEPES (HyClone #SH30023.01) with 10 mM HEPES (Sigma #H3537), 5% FBS, 1 mg/mL bovine serum albumin (BSA, Sigma #A7906), 1 µg/mL insulin (Invitrogen #51500-056), 0.5 µg/mL hydrocortisone (Sigma #H0888), 50 µg/mL gentamycin (HyClone #3V30080.01), and 2.5 µg/mL Fungizone. Primary human breast cell media was also prepared using EpiCult™-C Human Medium Kit (Stemcell™ Technologies #05630) by following the kit instructions for preparation of the complete EpiCult™-C Medium. Anti-CAR antibody (polyclonal, #PA5-110995) was purchased from Invitrogen, Anti-E-Cadherin antibody (clone 24E10, #3195P) was purchased from Cell Signaling Technology, and Anti-p120-Catenin (clone 98, #790–4517) was purchased from Roche Diagnostics. Anti-Rabbit HRP Polymer (#2RH-100) and Anti-Mouse HRP Polymer (#2MH-100) were obtained from Cell IDX. Tyramide-488 Reagent (#B40953), Tyramide-647 Reagent (#B40958), and Tyramide-594 Reagent (#B40957) were obtained from Thermo Fisher Scientific.

1.3.2 Synthesis of liposome-encapsulated Ad-GFP

Liposome-encapsulation of Ad was also performed by extrusion, which was described previously [28]. In brief, 1,2-dioleoyl-3-trimethylammonium-propane (DOTAP, Avanti #890890 C), cholesterol (Sigma #C3045), 1,2-distearoyl-sn-glycero-3-phosphoethanolamine-N-

[carboxy(polyethylene glycol)-2000] [PEG(2000)-PE carboxylic acid, Avanti #880124P], and 1,2-distearoyl-sn-glycero-3-phosphoethanolamine-N-[folate(polyethylene glycol)-2000] [PEG(2000)-Folate-PE, Avanti #880124P] were mixed together in chloroform at a molar ratio of 1:0.26:0.02:0.01. To make 400 uL of DOTAP-folate Ad-GFP (DfAd-GFP), 387 nmol of DOTAP, 100 nmol of Cholesterol, 7.01 nmol of PEG(2000)-PE carboxylic acid, and 3 nmol of PEG(2000)-folate-PE was added to 193.1 μL of chloroform (Sigma #C2432) in an amber vial (Fisher Scientific #03-339-23 C). The lipid mixture was vortexed for 30 min at 25 ℃. Subsequently, the mixture was vortexed in an amber vial for 30 min at room temperature. The resulting mixture was vacuumed overnight to form a dry lipid film at the bottom of the vial. The next day, the dry film was rehydrated with 400 uL of phosphate buffered saline (PBS, Fisher Scientific #10010072) while vortexing. The hydrated film was stirred at 600 rpm for 30 min at 4 ℃. Empty liposomes were formed by extruding the lipid mixture with the Avanti Mini Extruder (Avanti #6100009-1EA) through a 200 nm membrane (Cytiva/Whatman #10417004), 8 times at room temperature. To the empty liposomes, Ad-GFP was added, and the mixture was incubated at room temperature for 30 min to allow for encapsulation of the Ad-GFP, resulting in extruded DOTAP-folate Ad-GFP liposomes (DfAd-GFP). The resulting extruded DfAd-GFP has an Ad to DOTAP lipid ratio [Viral Particles (VP): nmol] of 5.17×10^7. For clarification, a large numerical value for this ratio does not signify an excess of viral particles relative to lipid nanoparticles; in fact, only ~ 10% of the liposomes encapsulate the virus [28].

1.3.3 Human breast cell isolation and culturing

Human breast tumor cell isolation and culturing was described previously [30]. Biospecimens were collected by the Moores Cancer Center Biorepository and Tissue technology shared resource from consented patients under a University of California, San Diego Human

Research Protections Program Institutional Research Board approved protocol (HRPP# 181755). Tumor fragments were acquired from two different areas of the same tumor when possible. During transportation, the acquired tumor tissues were placed in a 50 mL conical tube with sterile PBS such that the tissue sample was entirely submerged in PBS. 2 mg/mL of type 3 collagenase (Worthing #LS004182) and hyaluronidase (Sigma #H3884) 100 U/mL in human tumor digestion buffer were prepared. 10 mL per gram of tissue 10 mL of digestion buffer containing enzymes was added into a well in a 6-well plate. Tissue was placed into the well and minced until finely chopped. If needed, a syringe plunger was used to smash the tissue. The resultant tissue mixture was incubated at 37 ℃ and 5% CO2 with pipette mixing performed every 30 min until 5 h of digestion time. Tissue was also digested using the Miltenyi Biotec gentleMACS™ Octo Dissociator with Heaters following the protocol provided in the Human Tumor Dissociation Kit (#130-095-929). The "37C_h_TDK_3" program was selected on the Octo Dissociator instrument when starting the digestion.

After digestion, the tissue mixture was strained using a 100 μm strainer and the filtrate was centrifuged at 530 g at room temperature for 5 min to collect cells, and the supernatant was removed. If red cells were observed in the cell pellet, then 5–10 mL of ACK buffer (Quality Biological #118-156-101) was added and incubated for 3 min. Cells were centrifuged at 530 g at room temperature for 5 min, and the supernatant was removed. This step was repeated until the red blood cells in the pellet were not visible. The resultant cells were resuspended in 10 mL of PBS and centrifuged at 530 g at room temperature for 5 min. The resultant cells were resuspended in 1 mL of primary human breast cell medium, and an aliquot of 10 μL was used for cell counting. Cells were plated at 30,000 cells/well in a 96-well plate and incubated at 37 ℃ and 5% CO2. Viral infection was performed after cells attached to the well (24–48 h after plating).

1.3.4 In vitro transduction

Cells were plated at 3×10^4 cells/well in 96-well plates and incubated at 37 ℃ and 5% CO_2 in complete media. Viral infection was performed after cells attached to the well (24–48 h after plating). DfAd-GFP or Ad-GFP were added to the cells (day 1) and incubated at 37 ℃ and 5% CO_2. GFP fluorescence intensities were measured using a Tecan F PLEX Infinite 200 Pro microplate reader (Tecan Group Ltd., Männedorf, Switzerland) on day 4 for human primary breast cancer cells, MCF7, SUM44PE, and MDA-MB-231 cells.

1.3.5 Fluorescence microscopy

Cells transduced with DfAd-GFP or Ad-GFP were analyzed under a Keyance BZ-X710 microscope (KEYENCE CORPORATION OF AMERICA, IL, USA) with a GFP filter and 470/40 nm excitation wavelength, 525/50 nm emission wavelength and dichroic mirror wavelength of 495 nm. Comparative micrographs were captured using 2x and 20x objective lenses.

1.3.6 CAR expression analysis by immunohistochemistry

All formalin-fixed paraffin-embedded (FFPE) human breast cancer specimens were processed and stained by the Biorepository and Tissue Technology Shared Resources (BTTSR) at UCSD. Tissue samples were baked at 60 ℃ for 1 h. Tissue samples were cleaned and rehydrated through successive liquid dips: three times through xylene, two times through 100% ethanol, two times through 95% ethanol, two times in 70% ethanol, and one time in deionized water. Tissue samples underwent antigen retrieval in tris-based antigen unmasking solution (pH9, Vector Laboratories #H-3301) at 95 ℃ for 30 min. Immunohistochemical staining was performed on an Intellipath automated IHC stainer (Biocare Medical, LLC., CA, USA). Tissue samples were treated with Bloxall (Vector Laboratories, #SP-6000) peroxidase block for 10 min.

The tissues were washed two times with tris-buffered saline (TBST, Santa Cruz Biotechnology #sc-36231-1). Tissue samples were blocked with 3% donkey serum in TBST for 10 min. The tissues were treated with 1:50 diluted rabbit anti-CAR primary antibody for 1 h. Afterwards, the tissue samples were washed two times with TBST. Tissues were treated with anti-rabbit HRP polymer for 30 min. Afterwards, the tissue samples were washed twice with TBST. Tissue samples were treated with brown DAB chromagen (VWR #95041-478) for 5 min. Subsequently, Tissue samples were washed with deionized water twice. Afterwards, the tissues were counterstained with Mayer's Hematoxylin (Sigma #51275-500 ml) for 5 min. Tissue samples were then washed twice with TBST and once with deionized water. Tissues were then dehydrated, cleared, and mounted with a xylene based mounting mixture.

1.3.7 CAR expression analysis by immunohistochemistry

All formalin-fixed paraffin-embedded (FFPE) human breast cancer specimens were processed and stained by the Biorepository and Tissue Technology Shared Resources (BTTSR) at UCSD. Tissue samples were baked at 60 ℃ for 1 h. Tissue samples were cleaned and rehydrated through successive liquid dips: three times through xylene, two times through 100% ethanol, two times through 95% ethanol, two times in 70% ethanol, and one time in deionized water. Tissue samples underwent antigen retrieval in tris-based antigen unmasking solution (pH9, Vector Laboratories #H-3301) at 95 ℃ for 30 min. Immunohistochemical staining was performed on an Intellipath automated IHC stainer (Biocare Medical, LLC., CA, USA). Tissue samples were treated with Bloxall (Vector Laboratories, #SP-6000) peroxidase block for 10 min. The tissues were washed two times with tris-buffered saline (TBST, Santa Cruz Biotechnology #sc-36231-1). Tissue samples were blocked with 3% donkey serum in TBST for 10 min. The tissues were treated with 1:50 diluted rabbit anti-CAR primary antibody for 1 h. Afterwards, the

tissue samples were washed two times with TBST. Tissues were treated with anti-rabbit HRP polymer for 30 min. Afterwards, the tissue samples were washed twice with TBST. Tissue samples were treated with brown DAB chromagen (VWR #95041-478) for 5 min. Subsequently, Tissue samples were washed with deionized water twice. Afterwards, the tissues were counterstained with Mayer's Hematoxylin (Sigma #51275-500 ml) for 5 min. Tissue samples were then washed twice with TBST and once with deionized water. Tissues were then dehydrated, cleared, and mounted with a xylene based mounting mixture.

1.3.8 Spatial analysis of CAR, p-120 catenin, and E-cadherin by multiplexing immunofluorescence

Tissue samples were baked at 60 ℃ for 1 h. Tissue samples were cleaned and rehydrated through successive alcohol dips: three times through xylene, two times through 100% ethanol, two times through 95% ethanol, two times in 70% ethanol, and one time in deionized water. Tissue samples underwent antigen retrieval in citrate-based antigen unmasking solution (pH6, Vector Laboratories #H-3300) at 95 ℃ for 30 min. Immunohistochemical staining was performed on an Intellipath automated IHC stainer. Tissue samples were treated with Bloxall peroxidase block for 10 min. The tissues were washed two times with tris-buffered saline (TBST, Santa Cruz Biotechnology #sc-36231-1). Tissue samples were blocked with Blotto (Thermo Fisher Scientific, #PI37530) protein block for 10 min. Tissues were treated with 1:50 diluted rabbit anti-CAR primary antibody for 1 h. Tissue samples were washed twice with TBST. The tissues were treated with anti-rabbit HRP polymer for 30 min. Tissue samples were washed twice with TBST. Tissue samples were treated with Tyramide-488 Reagent for 10 min. The tissues were washed twice with deionized water. Tissues underwent another cycle of antigen retrieval in citrate-based antigen unmasking solution at 95 ℃ for 30 min.

Tissues were treated with Ready-to-use Mouse Anti-p120 Catenin Primary Antibody for 1 h. Tissue samples were washed twice with TBST. The tissues were treated with anti-rabbit HRP polymer for 30 min. Tissue samples were washed twice with TBST. Tissue samples were treated with Tyramide-647 Reagent for 10 min. Tissues underwent one last cycle of antigen retrieval in citrate-based antigen unmasking solution at 95 ℃ for 30 min. Tissues were treated with 1:2000 diluted anti-E-cadherin primary antibody for 1 h. Tissue samples were washed twice with TBST. The tissues were treated with anti-rabbit HRP polymer for 30 min. Tissue samples were washed twice with TBST. Tissue samples were treated with Tyramide-594 reagent for 10 min. The tissues were washed twice with deionized water. The tissue samples were counterstained with 1 µg/mL of DAPI for 5 min. Tissues were mounted with Vectashield Vibrance (Vector Laboratories #H-1700-10) cover slips.

1.4 Results

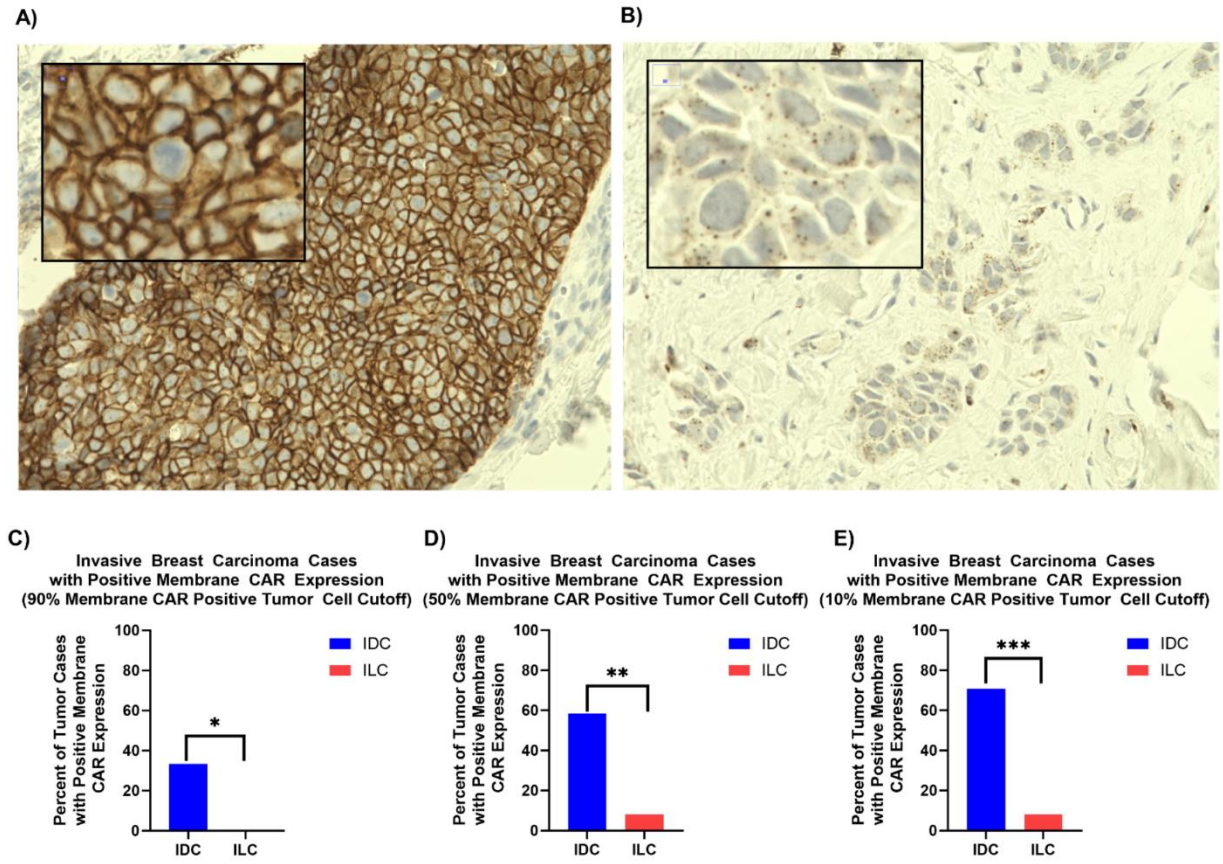

Figure 1.1 CAR expression in invasive breast cancer.
(A) This is an example IDC case with 3 + CAR staining intensity in the membrane of the tumor cells. (B) This is an example ILC case where there is no membrane CAR in the tumor cells. Instead, it presents dot-like CAR aggregates in the cytosol of the tumor cells. The staining is all located inside the cells and not the intracellular space. (C) At a 90% positive tumor cell cutoff, there were significantly greater IDC cases with positive membrane CAR expression compared to ILC cases. *$p < 0.05$. (D) At a 50% positive tumor cell cutoff, there were significantly greater IDC cases with positive membrane CAR expression compared to ILC cases. **$p < 0.005$. (E) At a 10% positive tumor cell cutoff, there were significantly greater IDC cases with positive membrane CAR expression compared to ILC cases. ***$p < 0.0005$

1.4.1 CAR expression analysis of invasive breast carcinoma

A total of 36 FFPE preserved patient breast cancer samples were obtained from BTTSR at UCSD. After hematoxylin and eosin (H&E) and CAR staining of the tissues, a pathologist diagnosed 24 cases as IDC and 12 cases as ILC. The pathologist also evaluated CAR expression,

staining intensity, and the percentage of CAR-expressing tumor cells. Two distinct localization patterns were observed for CAR: membranous and punctate cytoplasmic. (Figure 1.1A and B) Out of these two spatial expression patterns, IDC cases showed CAR expression mainly in the membrane of tumor cells while ILC cases showed punctate CAR staining within the cytoplasm. The IDC cases showed positive membrane staining in 50.7% of tumor cells while ILC cases showed positive membrane staining in only 7.2% of tumor cells. (Supplementary Figure 1.1) The percentage of tumor cells displaying CAR membrane expression in each case was further investigated and with a cutoff of 90% positive membrane-staining tumor cells, 33.3% of the IDC cases were positive for membranous CAR expression while none of the ILC cases were positive. (Fig. 1.1C) Even when the cutoff was set to 10%, only 8.3% of ILC cases were positive for membrane CAR expression while 70.8% of IDC cases were positive. (Fig. 1.1E) Therefore, the present study documents that IDC generally expresses CAR in the membrane of tumor cells while in ILC, CAR is expressed in the cytoplasm as dot-like aggregates.

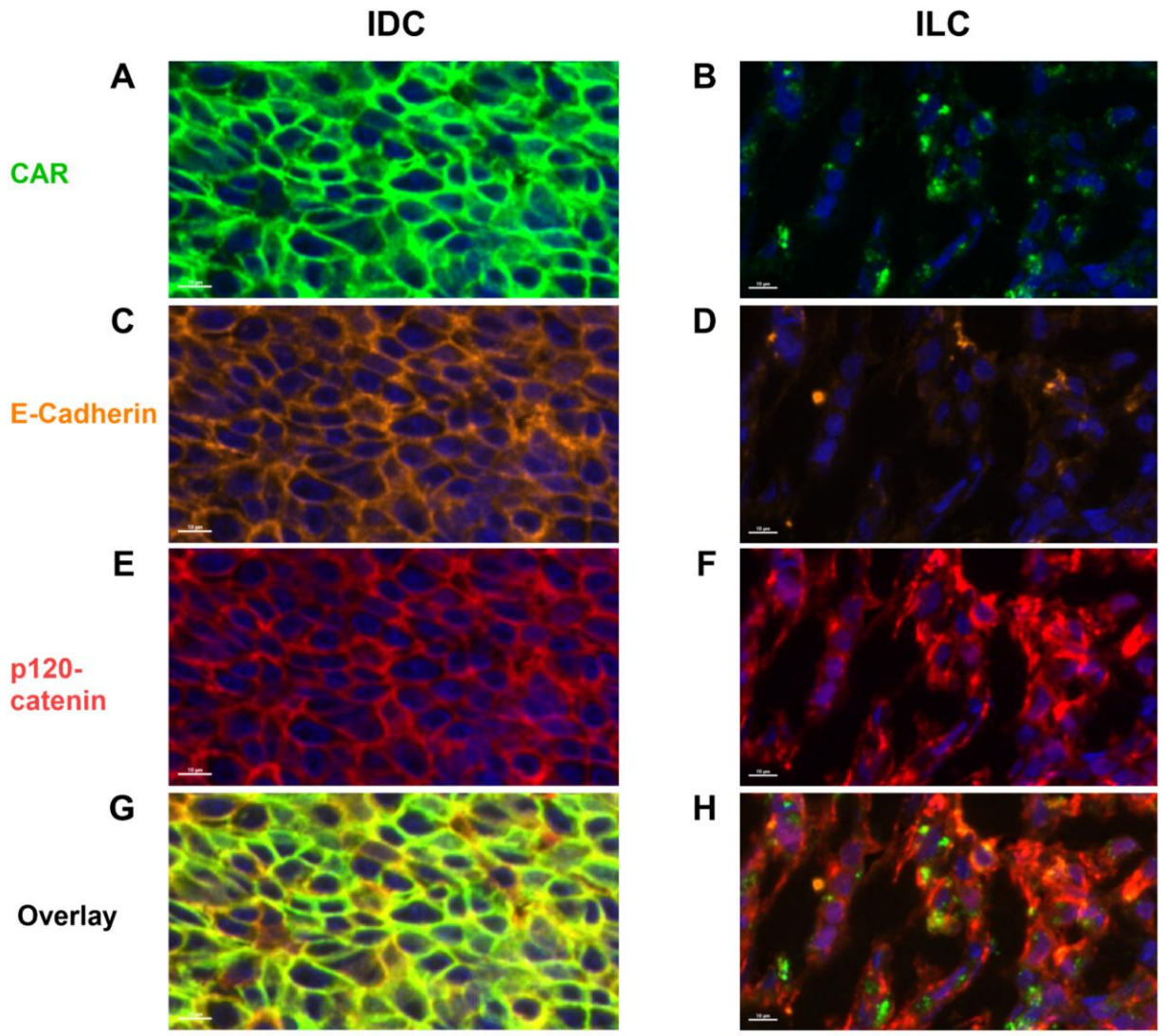

Figure 1.2 Co-expression of CAR, p120-Catenin, and E-Cadherin in invasive lobular carcinoma using multiplex immunofluorescence histology.
(A)(C)(E)(G) CAR in green, E-Cadherin in orange, p120-Catenin in red, and overlap fluorescent micrographs of a human IDC tumor sample, respectively. Note that all proteins are in the membrane of IDC tumor cells. Magnified 89.2x (B)(D)(F)(H) CAR in green, E-Cadherin in orange, p120-Catenin in red, and overlap fluorescent micrographs of a human ILC tumor sample, respectively. Note that both CAR and p120-catenin are in the cytoplasm of ILC tumor cells. Magnified 82.9x

1.4.2 Co-expression of CAR, E-cadherin, and p120-catenin

To investigate the spatial localization of CAR in relation to other junction proteins, three IDC and three ILC tissue blocks from the CAR expression analysis in Fig. 1.1 were sectioned

and assayed with a multiplex immunofluorescence panel of anti-CAR, anti-E-cadherin, and anti-p120-catenin antibodies. All three IDC cases demonstrated co-expression of CAR, E-cadherin, and p120-catenin in the membrane of tumor cells. An example of the membranous co-expression of all three biomarkers in IDC is shown in Fig. 1.2A, C and E, and G, and lower magnification images are shown in the supplement (Supp. Fig. 1.2A, C, E, G). In all three ILC cases, CAR and p120-catenin are both located in the cytoplasm; there is weak cytoplasmic fluorescence in the E-cadherin channel, but it may be attributed to bleed-through by the p120-catenin fluorophore (Fig. 1.2B, D and F, and H, and Supp. Fig. 1.2B, D, F, H).

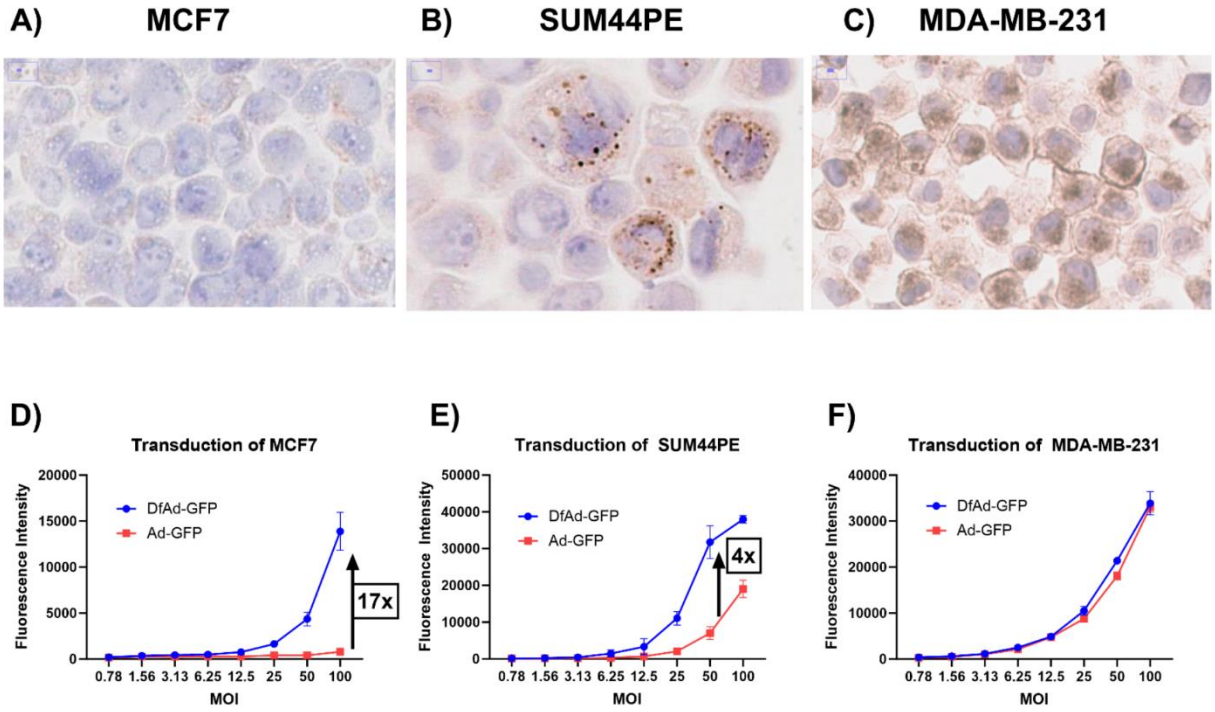

Figure 1.3 In vitro transduction of IDC and ILC cell lines.
(A) CAR IHC of MCF7 shows negative CAR expression in membrane and cytoplasm. (B) CAR IHC of SUM44PE shows negative CAR expression in membrane and punctate cytoplasmic expression. (C) CAR IHC of MDA-MB-231 shows positive CAR expression in membrane and some cytoplasmic expression. (D) Transduction efficiency of MCF7, a CAR-negative IDC cell line. (E) Transduction efficiency of SUM44PE, a membrane CAR-negative ILC cell line. (F) Transduction efficiency of MDA-MB-231, a membrane CAR-positive IDC cell line. Error bars are standard error of the mean (SEM)

1.4.3 Transduction of established IDC and ILC Cell lines with DfAd and Ad

To learn how CAR expression differences affect the transduction efficiency of each of the cell lines in this study, CAR IHC staining was performed on cell pellets of each of the cell lines. The cell lines used were MCF7, a CAR-negative IDC cell line, MDA-MB-231, a high-CAR IDC cell line and SUM44PE is an ILC cell line. CAR IHC staining reveals no CAR expression in either the membrane or cytoplasm in MCF7 (Fig. 1.3A). CAR expression is dot-like in the cytoplasm of SUM44PE similar to that observed in human ILC tissue specimens (Fig. 1.3B). CAR IHC staining of MDA-MB-231 demonstrated high CAR expression in the cell membrane similar to what was observed in human IDC tissue specimens (Fig. 1.3C). To model how DfAd and Ad transduce IDC and ILC tumor cells, MCF7, SUM44PE, and MDA-MB-231 cells were transduced by DfAd-GFP and Ad-GFP. MCF7 cells treated with DfAd-GFP at MOI 100 demonstrated 17-times higher transduction efficiency compared to cells treated by Ad-GFP at the same MOI (Fig. 1.3D). SUM44PE cells treated with DfAd-GFP at MOI 50 demonstrated 4-fold higher transduction efficiency compared to cells treated by Ad-GFP at the same MOI (Fig. 1.3E). MDA-MB-231 cells treated with DfAd-GFP demonstrated similar transduction efficiencies to cells treated by Ad-GFP at all MOIs (Fig. 1.3F).

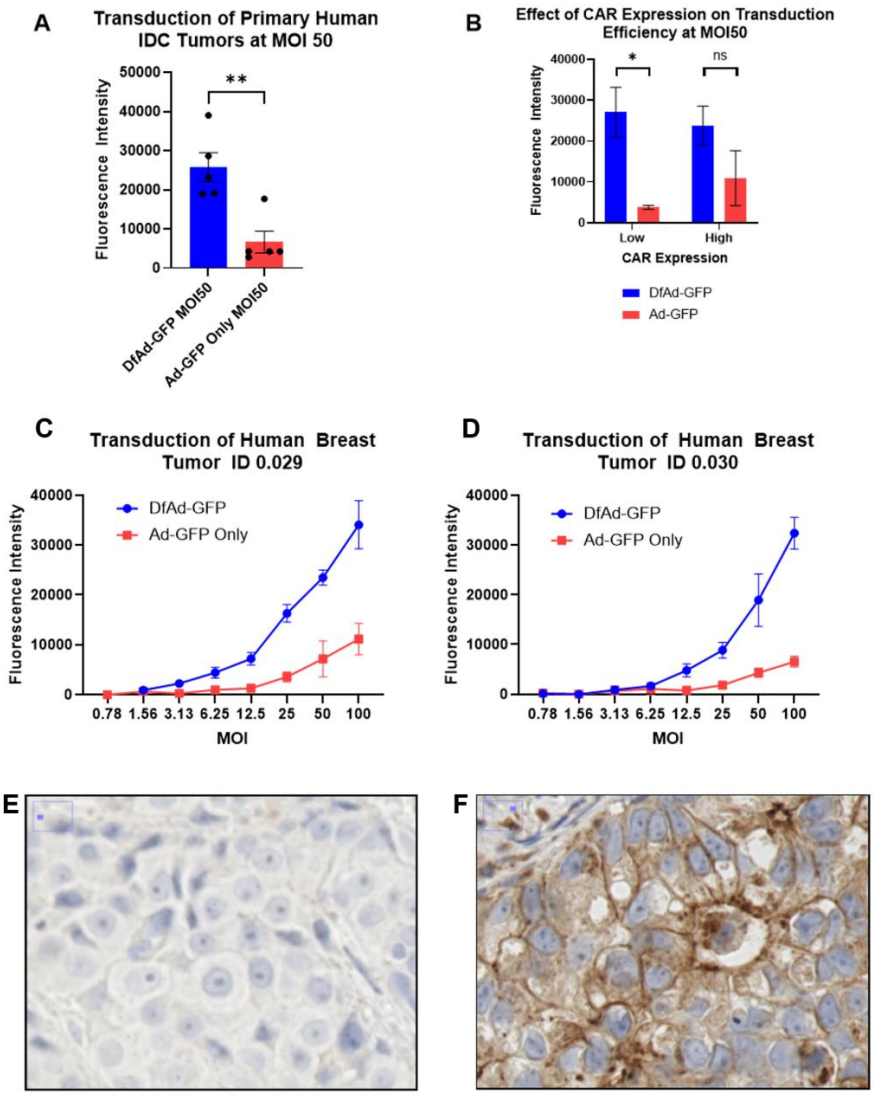

Figure 1.4 In vitro transduction of patient derived IDC tumor samples.
(A) The average transduction efficiency of primary human IDC tumors when transduced with DfAd-GFP versus Ad-GFP at MOI 50. n = 5, **p < 0.005 (B) Effect of CAR Expression on transduction efficiency of DfAd-GFP to Ad-GFP of primary human IDC tumors after batching cases with staining intensity 0–2 into "Low" CAR expression and 3 into "High" CAR Expression (n = 3 in Low and n = 2 in High), *p < 0.05, ns = not significant. (C) The transduction efficiency of primary human tumor sample ID 0.029 when transduced with DfAd-GFP versus Ad-GFP at multiple MOI. n = 3. (D) The transduction efficiency of primary human tumor sample ID 0.030 when transduced with DfAd-GFP versus Ad-GFP at multiple MOI. n = 3. Of the five reported tumor samples, 0.029 and 0.030 were the only two samples that yielded sufficient cells to measure transduction efficiency at multiple MOIs. (E) CAR IHC staining of an IDC tumor that shows CAR staining intensity < 1+. (F) CAR IHC staining of an IDC tumor that shows very high CAR staining intensity 3+. Error bars are SEM

1.4.4 Transduction of human primary IDC tumor cells

To model how DfAd and Ad transduce primary human breast tumors, human breast tumor samples were homogenized into single cells and transduced with DfAd-GFP and Ad-GFP. Data from five unique IDC tumor cases were collected by the end of this study. The average transduction efficiency of all five breast tumors treated with DfAd-GFP at MOI 50 was about 4-fold higher than when they were treated with Ad-GFP at MOI 50 (Fig. 1.4A). To learn how CAR expression differences affect the transduction efficiency of each of the breast tumor samples, a pathologist quantified the membranous and cytoplasmic CAR expression for each tumor sample by evaluating CAR IHC-stained tissues for each of the tumor cases. Human IDC tumor samples with low CAR expression demonstrated 7-fold higher transduction efficiency when treated with DfAd-GFP compared to when treated with Ad-GFP (Fig. 1.4B). However, human IDC tumor cases with high CAR expression only demonstrated 2-fold higher transduction efficiency when treated with DfAd-GFP compared to when the cells were treated with Ad-GFP, but this difference was not statistically significant (Fig. 1.4B). DfAd-GFP demonstrated higher transduction efficiency than Ad-GFP in two human breast tumor samples at MOI 12.5 or greater (Fig. 1.4C-D). IHC of one of the human primary IDC tumor samples with low CAR expression is shown in Fig. 1.4E. IHC of a tumor sample with high membranous CAR expression is shown in Fig. 1.4F. Unbinned data showing the transduction efficiencies and CAR staining intensities of each tumor case is shown in the supplement (Supp. Fig. 1.3).

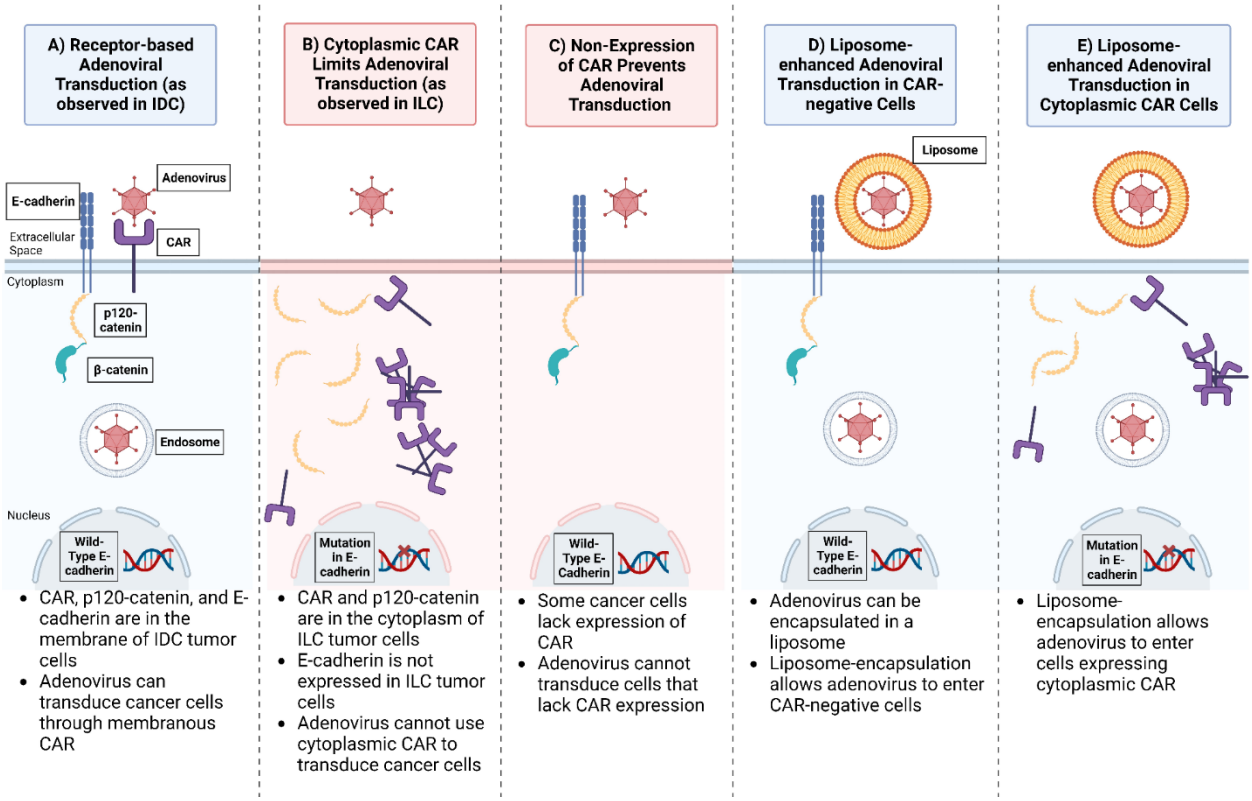

Figure 1.5 Schematic of adenoviral transduction and CAR-catenin-cadherin expression in invasive breast carcinoma.
(A) In IDC, wild-type E-cadherin is expressed in the membrane of breast cancer cells, and becomes complexed with p120-catenin and β-catenin. CAR is also expressed on the membrane of breast cancer cells. Breast cancer cells expressing membrane-bound CAR can be transduced by adenovirus through receptor-based transduction. (B) In ILC, the E-cadherin gene is mutated resulting in loss of expression of E-cadherin, resulting in p120-catenin translocation to the cytoplasm. CAR is also translocated to the cytoplasm. Breast cancer cells that only express cytosolic CAR cannot be transduced by the adenovirus. (C) Breast cancer cells that do not express any CAR cannot be transduced by adenovirus. This is the scenario when transducing ILC and IDC tumor cells that do not show CAR expression. (D) Without CAR expression, liposome encapsulation is used to allow adenovirus entry into the cell without needing CAR. (E) To enter cells expressing only cytoplasmic CAR, liposome encapsulation is used to allow adenovirus entry into the cell without needing membranous CAR

1.5 Discussion

CAR is a transmembrane protein and makes up tight junctions between epithelial cells as part of the junction adhesion molecules. While CAR expression in breast cancer has been previously studied, this study is the first report to demonstrate the spatial heterogeneity of CAR

in IDC and ILC, as well as dot-like, cytoplasmic spatial expression pattern of CAR in the ILC samples. Martin et al. measured CAR mRNA expression in various breast cancers by reverse transcription quantitative polymerase chain reaction (RT-qPCR) and found that ductal carcinoma showed elevated transcriptional CAR expression compared to lobular carcinoma [38]. Although they also show some micrographs of CAR IHC staining of breast tumor tissues, the lack of contrast between the CAR stain and the nuclear stain, and the grey scale coloration make the IHC results difficult to interpret [38]. Reeh et al. measured CAR expression by CAR IHC staining of microarrays in a broad range of tumors [41]. Despite having a larger sample size (n = 60 IDC and n = 64 ILC), they demonstrated much lower percentages of CAR positive IDC cases (8.3%) compared to the present study. (41) This discrepancy may be caused by heterogeneous expression of CAR in breast tumors as tissue microarrays (TMAs) only sample a small portion of each tumor block for interpretation. The advantage of whole tumor section evaluation is the potential to better interpret and evaluate heterogeneous tumors. It is noted that Reeh et al. used different antibodies and methodology for their IHC, potentially resulting in different tissue staining results. They also analyzed their pathology results using "immunoreactive score" instead of staining intensity, likely resulting in a different distribution of positive and negative cases. Furthermore, the Reeh study did not perform an in-depth analysis of CAR localization patterns in IDC compared to ILC as we have done in the present study.

One of the pathophysiological characteristics of ILC is the mutation in the CDH1 gene, resulting in the loss of E-cadherin expression in the epithelial cells [42, 43]. In response to this, p120-catenin translocates from the membrane to the cytoplasm, which initiates ILC tumor progression and increases tumor cell invasion [44,45,46,47]. Just as the loss of E-cadherin results in the

cytoplasmic localization of p120-catenin, we observed that the loss of E-cadherin in the ILC correlates with the cytoplasmic localization of CAR (illustrated in Fig. 1.5). Previous studies investigated how CAR regulates E-cadherin stability in model cell lines in vitro [48, 49], however, our study is the first to show that the loss of E-cadherin, as observed in ILC, affects CAR localization. Supp. Fig. 1.4 summarizes how membrane expression levels of CAR, E-cadherin, and p120-catenin differ between IDC and ILC.

Using cell lines MCF7 and MDA-MB-231 to model IDC with no CAR expression and high membrane CAR expression, respectively, we show that liposome encapsulation (DfAd-GFP) increases adenoviral transduction efficiency up to 17-fold in CAR negative cells. In contrast, the high-CAR cell line, MDA-MB-231 showed no change in transduction efficiency by liposome encapsulation as Ad-GFP could already enter the cells efficiently through the CAR receptor. Previous literature had used other CAR-negative and CAR-positive IDC cell lines to evaluate DfAd and Ad transduction efficiency. (28–30) However, no previous studies had modeled DfAd and Ad transduction in ILC cell lines. Our experiments using SUM44PE, an ILC cell line, showed 4-fold enhanced transduction efficiency using DfAd-GFP compared to Ad-GFP, indicating that liposome enhanced transduction is more efficient in ILC tumor cells than receptor-based Ad transduction through CAR. In primary human IDC tumor samples, DfAd-GFP demonstrated 4-fold higher transduction efficiency compared to the Ad-GFP, indicating that liposome encapsulation can improve Ad transduction in human IDC tumor cells. This differential may improve adenoviral mediated therapy for human breast tumors. Our study was limited by the absence of primary ILC tumor specimens; we plan future studies using human ILC patient-derived xenograft models in mice to study the treatment of human ILC using liposome-encapsulated adenoviral therapy.

1.6 Conclusion

Oncolytic adenoviral therapy is a potentially promising therapeutic option for breast cancer patients. The present study demonstrated that the two major subtypes of invasive breast carcinoma, IDC and ILC, differ significantly in terms of spatial expression of CAR and adenoviral transduction efficiency, which may impact the efficacy of adenoviral-based therapeutics. While IDC tumors typically express CAR in the membrane of tumor cells, ILC tumors express CAR mainly in the cytoplasm. We show that liposome encapsulation improves adenoviral transduction in ILC cell lines expressing cytoplasmic CAR. We also observed that in human primary breast cancer cells, liposome encapsulation (DfAd) demonstrated higher transduction efficiency compared to unencapsulated adenovirus (Ad). The present study also showed a correlation between CAR, E-cadherin, and p120-catenin in IDC and ILC in human breast cancer tissue, which suggests an interdependency of tight and adherens junction proteins. Overall, our study suggests that adenoviral therapy would most likely benefit patients with CAR-positive IDC tumors, while liposome-enhanced adenoviral delivery would be needed patients with ILC or CAR-negative IDC. This novel immunotherapy extends therapeutic opportunities for ILC patients which primarily consists of hormonal therapy at present and has the potential for rapid translation to clinical use.

1.7 Acknowledgements

Chapter 1, in full, is a reprint of the material as it appears in Breast Cancer Research 2024. Phung, Abraham T.; Shah, Jaimin R.; Dong, Tao; Reid, Tony; Larson, Christopher; Sanchez, Ana B.; Oronsky, Bryan; Trogler, William C.; Kummel, Andrew C.; Aisagbonhi, Omonigho; Blair, Sarah L. Springer Nature, 2024. The dissertation author was the primary author of this paper.

1.8 Supplementary Material

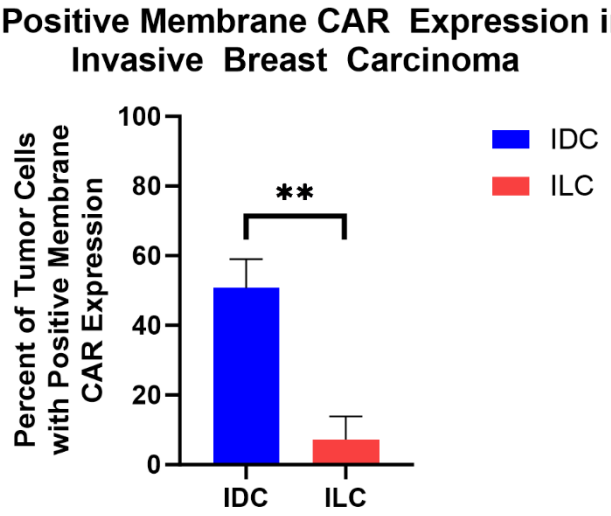

Supplementary Figure 1.1 CAR Expression in Invasive Breast Cancer based on Positive Tumor Cell Percentage.
IDC tumors, on average, showed significantly higher percentages of tumor cells that stained for CAR at 1-3+ intensity in the membrane compared to ILC tumors. **p<0.005. Error bars are SEM.

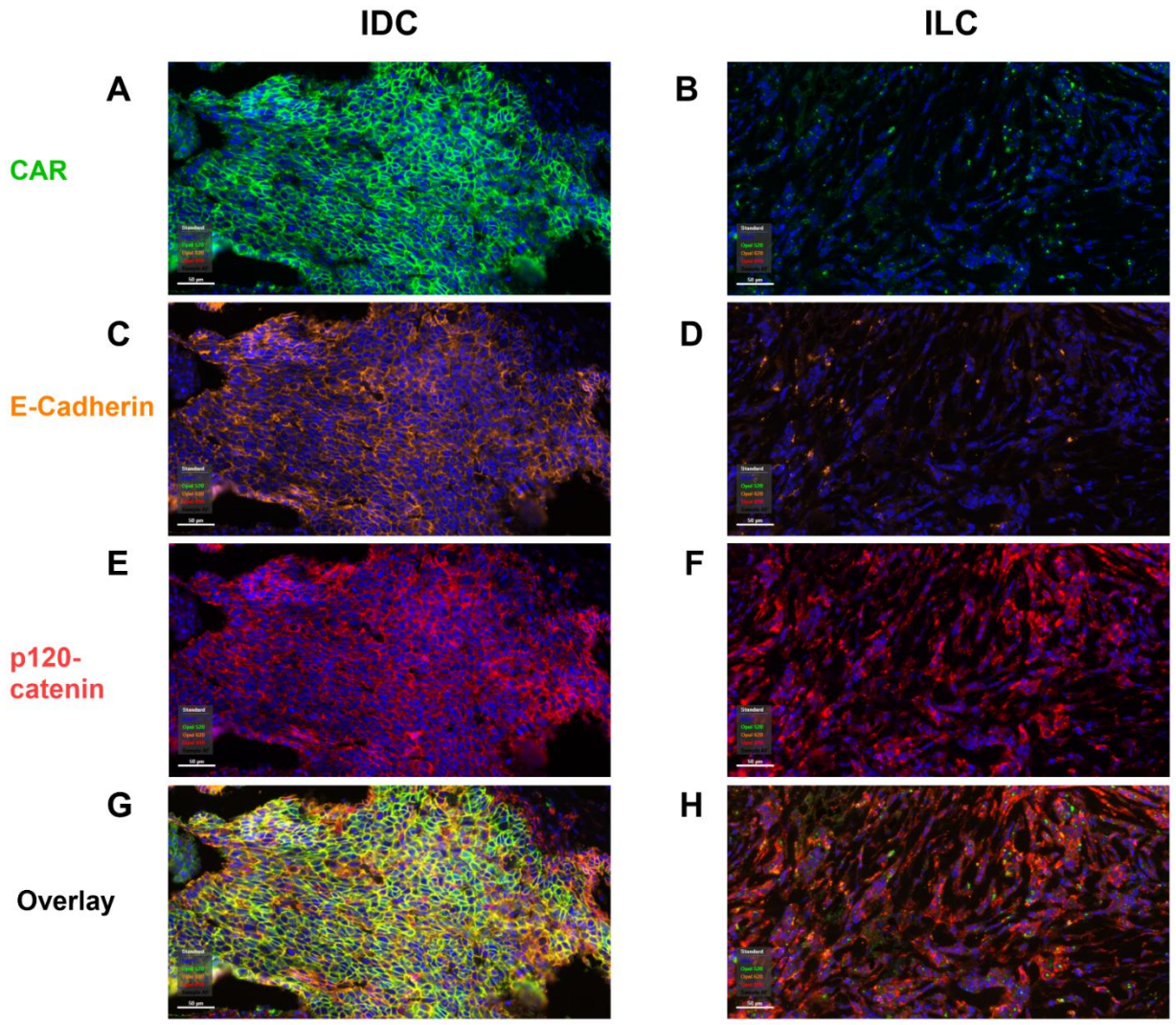

Supplementary Figure 1.2 (Zoomed Out) Co-Expression of CAR, p120-Catenin, and E-Cadherin in Invasive Lobular Carcinoma using Multiplex Immunofluorescence Histology. (A)(C)(E)(G) CAR, p120-Catenin, E-Cadherin, and overlap fluorescent micrographs of a human IDC tumor sample, respectively. (B)(D)(F)(H) CAR, p120-Catenin, E-Cadherin, and overlap fluorescent micrographs of a human ILC tumor sample, respectively.

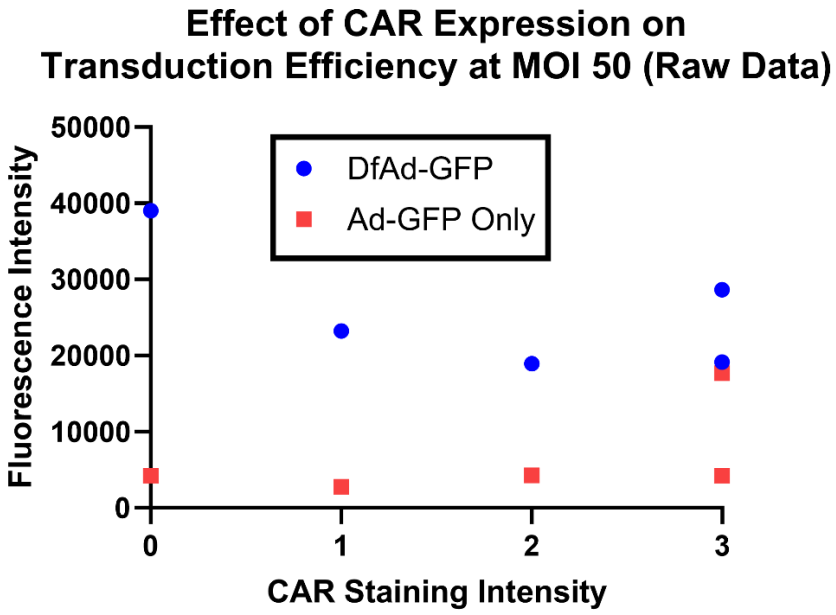

Supplementary Figure 1.3 Effect of CAR Expression on the transduction efficiency of primary human IDC tumors

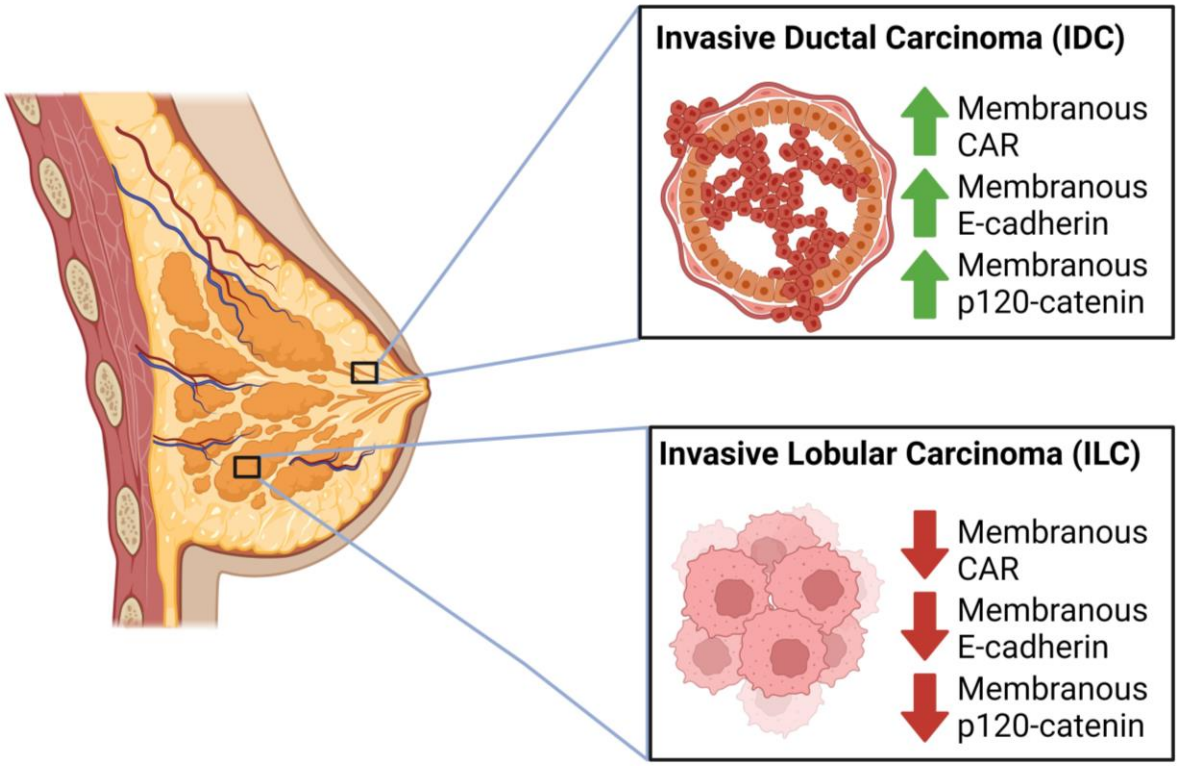

Supplementary Figure 1.4 Summary of pathological characteristics of invasive breast carcinoma.
IDC typically demonstrates positive E-cadherin and p120-catenin in the membranes of tumor cells. ILC is pathologically characterized by loss of expression of E-cadherin and loss of expression or translocation of p120-catenin to the cytosol. CAR expression analysis using immunohistochemistry reveals the IDC also typically expresses membranous CAR while in ILC, CAR expression is either completely lost or it is translocated to the cytosol.

1.9 References

1. Chamalidou, C.; Fohlin, H.; Albertsson, P.; Arnesson, L.-G.; Einbeigi, Z.; Holmberg, E.; Nordenskjöld, A.; Nordenskjöld, B.; Karlsson, P.; Linderholm, B. Survival patterns of invasive lobular and invasive ductal breast cancer in a large population-based cohort with two decades of follow up. The Breast 2021, 59, 294-300, doi:10.1016/j.breast.2021.07.011.

2. Wilson, N.; Ironside, A.; Diana, A.; Oikonomidou, O. Lobular Breast Cancer: A Review. Frontiers in Oncology 2021, 10, doi:10.3389/fonc.2020.591399.

3. Du, T.; Zhu, L.; Levine, K.M.; Tasdemir, N.; Lee, A.V.; Vignali, D.A.A.; Houten, B.V.; Tseng, G.C.; Oesterreich, S. Invasive lobular and ductal breast carcinoma differ in immune response, protein translation efficiency and metabolism. Scientific Reports 2018, 8, doi:10.1038/s41598-018-25357-0.

4. Oesterreich, S.; Nasrazadani, A.; Zou, J.; Carleton, N.; Onger, T.; Wright, M.D.; Li, Y.; Demanelis, K.; Ramaswamy, B.; Tseng, G.; Lee, A.V.; Williams, N.; Kruse, M. Clinicopathological Features and Outcomes Comparing Patients With Invasive Ductal and Lobular Breast Cancer. JNCI: Journal of the National Cancer Institute 2022, 114, 1511-1522, doi:10.1093/jnci/djac157.

5. Pestalozzi, B.C.; Zahrieh, D.; Mallon, E.; Gusterson, B.A.; Price, K.N.; Gelber, R.D.; Holmberg, S.B.; Lindtner, J.; Snyder, R.; Thürlimann, B.; Murray, E.; Viale, G; Vastiglione-Gertsch, M.; Coates, A.S.; Goldhirsch, A. Distinct Clinical and Prognostic Features of Infiltrating Lobular Carcinoma of the Breast: Combined Results of 15 International Breast Cancer Study Group Clinical Trials. Journal of Clinical Oncology 2008, 26, 3006-3014, doi:10.1200/jco.2007.14.9336.

6. Chumsri, S.; Li, Z.; Shachner, T.; Advani, P.; Sideras, K.; Moreno-Aspitia, A.; Colon-Otero, G.; Knutson, K.L.; Nassar, A.; Perez, E.A.; Thompson, E.A. Outcome and immune landscape of HER2-positive invasive lobular carcinoma in the North Central Cancer Treatment Group (NCCTG) N9831 (Alliance) trial. Journal of Clinical Oncology 2021, 39, 535-535, doi:10.1200/JCO.2021.39.15_suppl.535.

7. Yang, C.; Lei, C.; Zhang, Y.; Zhang, J.; Ji, F.; Pan, W.; Zhang, L.; Gao, H.; Yang, M.; Li, J.; Wang, K. Comparison of Overall Survival Between Invasive Lobular Breast Carcinoma and Invasive Ductal Breast Carcinoma: A Propensity Score Matching Study Based on SEER Database. Front Oncol 2020, 10, 590643, doi:10.3389/fonc.2020.590643.

8. Engstrøm, M.J.; Opdahl, S.; Vatten, L.J.; Haugen, O.A.; Bofin, A.M. Invasive lobular breast cancer: the prognostic impact of histopathological grade, E-cadherin and molecular subtypes. Histopathology 2015, 66, 409-419, doi:https://doi.org/10.1111/his.12572.

9. Luo, Y.; Ma, A.; Huang, S.; Yu, Y. Invasive Lobular Carcinoma Has Worse Outcome Compared with Invasive Ductal Carcinoma in Stage IV Breast Cancer with Bone-Only Metastasis. Breast Care 2022, 17, 296-305, doi:10.1159/000521097.

10. Bommareddy, P.K.; Patel, A.; Hossain, S.; Kaufman, H.L. Talimogene Laherparepvec (T-VEC) and Other Oncolytic Viruses for the Treatment of Melanoma. American Journal of Clinical Dermatology 2017, 18, 1-15, doi:10.1007/s40257-016-0238-9.

11. Howells, A.; Marelli, G.; Lemoine, N.R.; Wang, Y. Oncolytic Viruses—Interaction of Virus and Tumor Cells in the Battle to Eliminate Cancer. Frontiers in Oncology 2017, 7, doi:10.3389/fonc.2017.00195.

12. Jayawardena, N.; Burga, L.N.; Poirier, J.T.; Bostina, M. Virus–Receptor Interactions: Structural Insights For Oncolytic Virus Development. Oncolytic Virotherapy 2019, Volume 8, 39-56, doi:10.2147/ov.s218494.

13. Carter, M.E.; Koch, A.; Lauer, U.M.; Hartkopf, A.D. Clinical Trials of Oncolytic Viruses in Breast Cancer. Frontiers in Oncology 2021, 11, doi:10.3389/fonc.2021.803050.

14. Ang, L.; Guo, L.; Wang, J.; Huang, J.; Lou, X.; Zhao, M. Oncolytic virotherapy armed with an engineered interfering lncRNA exhibits antitumor activity by blocking the epithelial mesenchymal transition in triple-negative breast cancer. Cancer Letters 2020, 479, 42-53, doi:10.1016/j.canlet.2020.03.012.

15. Aldrak, N.; Alsaab, S.; Algethami, A.; Bhere, D.; Wakimoto, H.; Shah, K.; Alomary, M.N.; Zaidan, N. Oncolytic Herpes Simplex Virus-Based Therapies for Cancer. Cells 2021, 10, 1541, doi:10.3390/cells10061541.

16. Matsumura, S.; Nakamori, M.; Tsuji, T.; Kato, T.; Nakamura, M.; Ojima, T.; Fukuhara, H.; Ino, Y.; Todo, T.; Yamaue, H. Oncolytic virotherapy with SOCS3 enhances viral replicative potency and oncolysis for gastric cancer. Oncotarget 2021, 12, 344-354, doi:10.18632/oncotarget.27873.

17. Gonzalez-Pastor, R.; Goedegebuure, P.S.; Curiel, D.T. Understanding and addressing barriers to successful adenovirus-based virotherapy for ovarian cancer. Cancer Gene Therapy 2021, 28, 375-389, doi:10.1038/s41417-020-00227-y.

18. Manyam, M.; Stephens, A.J.; Kennard, J.A.; LeBlanc, J.; Ahmad, S.; Kendrick, J.E.; Holloway, R.W. A phase 1b study of intraperitoneal oncolytic viral immunotherapy in platinum-resistant or refractory ovarian cancer. Gynecologic Oncology 2021, 163, 481-489, doi:10.1016/j.ygyno.2021.10.069.

19. Suryawanshi, Y.R.; Schulze, A.J. Oncolytic Viruses for Malignant Glioma: On the Verge of Success? Viruses 2021, 13, 1294, doi:10.3390/v13071294.

20. Todo, T.; Ito, H.; Ino, Y.; Ohtsu, H.; Ota, Y.; Shibahara, J.; Tanaka, M. Intratumoral oncolytic herpes virus G47Δ for residual or recurrent glioblastoma: a phase 2 trial. Nature Medicine 2022, 28, 1630-1639, doi:10.1038/s41591-022-01897-x.

21. Special Combination of OBP-301 and Pembrolizumab.

22. Phase I Dose Escalation Study of Intravenous VCN-01 With or Without Gemcitabine and Abraxane® in Patients With Advanced Solid Tumors.

23. Phase I Endovenous Administration of Oncolytic Adenovirus ICOVIR-5 in Patients With Advanced or Metastatic Melanoma.

24. Larson, C.; Oronsky, B.; Reid, T. AdAPT-001, an oncolytic adenovirus armed with a TGF-β trap, overcomes in vivo resistance to PD-L1-immunotherapy. Am J Cancer Res 2022, 12, 3141-3147.

25. Wunder, T.; Schmid, K.; Wicklein, D.; Groitl, P.; Dobner, T.; Lange, T.; Anders, M.; Schumacher, U. Expression of the coxsackie adenovirus receptor in neuroendocrine lung cancers and its implications for oncolytic adenoviral infection. Cancer Gene Therapy 2013, 20, 25-32, doi:10.1038/cgt.2012.80.

26. Hensen, L.C.M.; Hoeben, R.C.; Bots, S.T.F. Adenovirus Receptor Expression in Cancer and Its Multifaceted Role in Oncolytic Adenovirus Therapy. International Journal of Molecular Sciences 2020, 21, 6828, doi:10.3390/ijms21186828.

27. Mendez, N.; Herrera, V.; Zhang, L.; Hedjran, F.; Feuer, R.; Blair, S.L.; Trogler, W.C.; Reid, T.R.; Kummel, A.C. Encapsulation of adenovirus serotype 5 in anionic lecithin liposomes using a bead-based immunoprecipitation technique enhances transfection efficiency. Biomaterials 2014, 35, 9554-9561, doi:10.1016/j.biomaterials.2014.08.010.

28. Shah, J.R.; Dong, T.; Phung, A.T.; Reid, T.; Larson, C.; Sanchez, A.B.; Oronsky, B.; Blair, S.L.; Aisagbonhi, O.; Trogler, W.C.; Kummel, A.C. Development of Adenovirus Containing Liposomes Produced by Extrusion vs. Homogenization: A Comparison for Scale-Up Purposes. Bioengineering 2022, 9, 620, doi:10.3390/bioengineering9110620.

29. Dong, T.; Shah, J.R.; Phung, A.T.; Larson, C.; Sanchez, A.B.; Aisagbonhi, O.; Blair, S.L.; Oronsky, B.; Trogler, W.C.; Reid, T.; Kummel, A.C. A Local and Abscopal Effect Observed with Liposomal Encapsulation of Intratumorally Injected Oncolytic Adenoviral Therapy. Cancers 2023, 15, 3157, doi:10.3390/cancers15123157.

30. Huang, C.-H.; Dong, T.; Phung, A.T.; Shah, J.R.; Larson, C.; Sanchez, A.B.; Blair, S.L.; Oronsky, B.; Trogler, W.C.; Reid, T.; Kummel, A.C. Full Remission of CAR-Deficient Tumors by DOTAP-Folate Liposome Encapsulation of Adenovirus. ACS Biomaterials Science & Engineering 2022, 8, 5199-5209, doi:10.1021/acsbiomaterials.2c00966.

31. Yang, M.; Yang, C.S.; Guo, W.; Tang, J.; Huang, Q.; Feng, S.; Jiang, A.; Xu, X.; Jiang, G.; Liu, Y.Q. A novel fiber chimeric conditionally replicative adenovirus-Ad5/F35 for tumor therapy. Cancer Biology & Therapy 2017, 18, 833-840, doi:10.1080/15384047.2017.1395115.

32. Cationic Liposomes Enhance Adenovirus Entry via a Pathway Independent of the Fiber Receptor and αv-Integrins. Human Gene Therapy 1998, 9, 507-520, doi:10.1089/hum.1998.9.4-507.

33. Yotnda, P.; Chen, D.-H.; Chiu, W.; Piedra, P.A.; Davis, A.; Templeton, N.S.; Brenner, M.K. Bilamellar Cationic Liposomes Protect Adenovectors from Preexisting Humoral Immune Responses. Molecular Therapy 2002, 5, 233-241, doi:10.1006/mthe.2002.0545.

34. Liu, S.-H.; Smyth-Templeton, N.; Davis, A.R.; Davis, E.A.; Ballian, N.; Li, M.; Liu, H.; Fisher, W.; Brunicardi, F.C. Multiple treatment cycles of liposome-encapsulated adenoviral RIP-TK gene therapy effectively ablate human pancreatic cancer cells in SCID mice. Surgery 2011, 149, 484-495, doi:10.1016/j.surg.2010.11.014.

35. Zhang, Y.; Wu, J.; Zhang, H.; Wei, J.; Wu, J. Extracellular Vesicles-Mimetic Encapsulation Improves Oncolytic Viro-Immunotherapy in Tumors With Low Coxsackie and Adenovirus Receptor. Frontiers in Bioengineering and Biotechnology 2020, 8, doi:10.3389/fbioe.2020.574007.

36. Yang, L.; Wang, L.; Su, X.-Q.; Wang, L.; Chen, X.-C.; Li, D.; Luo, S.-T.; Shi, H.-S.; Chen, L.-J.; Wang, Y.-S. Suppression of ovarian cancer growth via systemic administration with liposome-encapsulated adenovirus-encoding endostatin. Cancer Gene Therapy 2010, 17, 49-57, doi:10.1038/cgt.2009.47.

37. Shi, H.-S.; Yang, L.-P.; Wei, W.; Su, X.-Q.; Li, X.-P.; Li, M.; Luo, S.-T.; Zhang, H.-L.; Lu, L.; Mao, Y.-Q.; Kan, B; Yang, L. Systemically administered liposome-encapsulated Ad-PEDF potentiates the anti-cancer effects in mouse lung metastasis melanoma. Journal of Translational Medicine 2013, 11, 86, doi:10.1186/1479-5876-11-86.

38. Martin, T.A.; Watkins, G.; Jiang, W.G. The Coxsackie-adenovirus receptor has elevated expression in human breast cancer. Clinical and Experimental Medicine 2005, 5, 122-128, doi:10.1007/s10238-005-0076-1.

39. Vindrieux, D.; Le Corre, L.; Hsieh, J.-T.; Métivier, R.; Escobar, P.; Caicedo, A.; Brigitte, M.; Lazennec, G. Coxsackie and adenovirus receptor is a target and a mediator of estrogen action in breast cancer. Endocrine-Related Cancer 2011, 18, 311-321, doi:10.1530/erc-10-0230.

40. Mach, N.; Gao, J.; Schaffarczyk, L.; Janz, S.; Ehrke-Schulz, E.; Dittmar, T.; Ehrhardt, A.; Zhang, W. Spectrum-Wide Exploration of Human Adenoviruses for Breast Cancer Therapy. Cancers 2020, 12, 1403, doi:10.3390/cancers12061403.

41. Reeh, M.; Bockhorn, M.; Görgens, D.; Vieth, M.; Hoffmann, T.; Simon, R.; Izbicki, J.R.; Sauter, G.; Schumacher, U.; Anders, M. Presence of the Coxsackievirus and Adenovirus Receptor (CAR) in human neoplasms: a multitumour array analysis. British Journal of Cancer 2013, 109, 1848-1858, doi:10.1038/bjc.2013.509.

42. Reed, A.E.M.; Kutasovic, J.R.; Lakhani, S.R.; Simpson, P.T. Invasive lobular carcinoma of the breast: morphology, biomarkers and 'omics. Breast Cancer Research 2015, 17, 12, doi:10.1186/s13058-015-0519-x.

43. Bajrami, I.; Marlow, R.; Van De Ven, M.; Brough, R.; Pemberton, H.N.; Frankum, J.; Song, F.; Rafiq, R.; Konde, A.; Krastev, D.B.; Menon, M.; Campbell, J.; Gulati, A.; Kumar, R.; Pettitt, S.J.; Gurden, M.D.; Cardenosa, M.L.; Chong, I.; Gazinska, P.; Wallberg, F.; Sawyer, E.J.; Martin, L.-A.; Dowsett, M.; Lindardopoulos, S.; Natrajan, R.; Ryan, C.J.; Derksen, P.W.B.; Jonkers, J.; Tutt, A.N.J.; Ashworth, A.; Lord, C.J. E-Cadherin/ROS1 Inhibitor Synthetic Lethality in Breast Cancer. Cancer Discovery 2018, 8, 498-515, doi:10.1158/2159-8290.cd-17-0603.

44. El Sharouni, M.-A.; Postma, E.L.; Van Diest, P.J. Correlation between E-cadherin and p120 expression in invasive ductal breast cancer with a lobular component and MRI findings. Virchows Archiv 2017, 471, 707-712, doi:10.1007/s00428-017-2203-2.

45. Kourtidis, A.; Ngok, S.P.; Anastasiadis, P.Z. p120 Catenin. In Progress in Molecular Biology and Translational Science; Elsevier: 2013; pp. 409-432.

46. Schackmann, R.C.J.; Van Amersfoort, M.; Haarhuis, J.H.I.; Vlug, E.J.; Halim, V.A.; Roodhart, J.M.L.; Vermaat, J.S.; Voest, E.E.; Van Der Groep, P.; Van Diest, P.J.; Jonkers, J.; Derksen, P.W.B. Cytosolic p120-catenin regulates growth of metastatic lobular carcinoma through Rock1-mediated anoikis resistance. Journal of Clinical Investigation 2011, 121, 3176-3188, doi:10.1172/jci41695.

47. Sarrió, D.; Pérez-Mies, B.; Hardisson, D.; Moreno-Bueno, G.; Suárez, A.; Cano, A.; Martín-Pérez, J.; Gamallo, C.; Palacios, J. Cytoplasmic localization of p120ctn and E-cadherin loss characterize lobular breast carcinoma from preinvasive to metastatic lesions. Oncogene 2004, 23, 3272-3283, doi:10.1038/sj.onc.1207439.

48. Morton, P.E.; Hicks, A.; Nastos, T.; Santis, G.; Parsons, M. CAR regulates epithelial cell junction stability through control of E-cadherin trafficking. Scientific Reports 2013, 3, doi:10.1038/srep02889.

49. Hussain, F.; Morton, P.E.; Snippe, M.; Sullivan, J.; Farmer, C.; Martin-Fernandez, M.L.; Parsons, M.; Santis, G. CAR Modulates E-Cadherin Dynamics in the Presence of Adenovirus Type 5. PLoS ONE 2011, 6, e23056, doi:10.1371/journal.pone.0023056.

Chapter 2 Adenoviruses Encapsulated in PEGylated DOTAP-Folate Liposomes Are Protected from the Pre-Existing Humoral Immune Response

2.1 Abstract

While adenovirus (Ad) therapies have been proven to be effective in local administration, systemic Ad treatments have shown limited success due to pre-existing antibodies in the human blood that neutralize the virus. We developed a liposome coating procedure that protects the Ad from pre-existing neutralizing antibodies in human blood. To assess the in vivo stability of the liposomes, the present study used a novel in vivo method to quantitatively assess the protective capabilities of liposome-encapsulated Ad (DfAd) from neutralizing antibodies. The assay systemically administers DfAd with a green fluorescent protein transgene (DfAd-GFP) into pre-immunized mice and allows it to circulate in the presence of neutralizing antibodies; the infected blood is extracted and used to transduce HEK293 cells, which emits fluorescence in the presence of protected, un-neutralized Ad. The PEGylated liposome formulation provides 12× protection in vivo relative to unencapsulated Ads. In vitro optimization of the liposome coating reveals a strong correlation between the structural stability of liposomes and protection against anti-Ad neutralizing antibodies, where DSPE-PEG2000-carboxylic acid (DSPE-PEG2000-CA) is a critical component for liposome stability and increasing protection against antibody neutralization of the encapsulated Ad. The findings in the present study confirm that the DfAd liposome can protect against neutralizing antibodies in blood circulation. The novel in vivo assay for liposome protection against neutralizing antibodies and in vitro experiments in the present study provide new tools and insights toward designing liposome–Ad complexes for the systemic treatment of cancer.

2.2 Introduction

Oncolytic adenovirus (Ad) therapy is an emerging treatment for various cancers, including, but not limited to, breast [1,2,3], gastrointestinal [4], ovarian [5], and brain cancers [6]. The treatment involves infecting and killing cancer cells with an Ad engineered to conditionally replicate in cancer cells, thereby inducing cell death but remaining harmless to healthy cells. When administered intratumorally, oncolytic adenoviral therapy effectively trains the immune system to identify and kill disseminating tumor cells and metastatic tumors [7]. The anti-tumor immune response can also be amplified by engineering the oncolytic Ad genome with a highly expressible transgene, such as immune stimulatory peptides [8], or combining intratumorally administered oncolytic Ad treatment with immune-checkpoint inhibitors (ICI) [9]. While these approaches theoretically treat both the primary and distant lesions, recent studies show tumors that regress from direct treatment with oncolytic viruses respond better to treatment than distant tumors that only regress from anti-tumor immunity [10,11]. Although studies of intratumoral delivery of oncolytic Ad have successfully regressed not only the injected primary tumor but also distant, noninjected tumors, intravenous administration is still the ideal route of treatment for hard to reach tumors and multiple tumors at the same time [12]. In summary, systemic delivery of oncolytic viruses may be the best approach to controlling local tumor lesions and metastatic disease compared with intratumoral delivery [13].

Current endeavors to systemically administer oncolytic Ad face many challenges, including dilution, opsonization, and neutralization [10,14,15]. Intravenous administration of oncolytic Ad significantly dilutes the administered dose. In conjunction with pre-existing humoral immunity against Ads in humans and liver macrophages that actively sequester foreign viral particles, the efficacy of systemically administered oncolytic Ad is greatly reduced by the

lack of viable virions reaching the target tumor site. Previous dose escalation studies showed that high-dose intravenous administration of oncolytic Ad is well tolerated, with no dose-limiting toxicities observed; however, in a few cases, flu-like symptoms have been observed [16,17,18]. Despite high-dose intravenous administration, these studies still showed low uptake of viral particles, with most of the virus being neutralized or sequestered by the liver [16,17,18,19,20,21]. Therefore, solutions to prevent adenoviral neutralization are critical for the clinical translation of systemically administered oncolytic viral therapy. One approach is to protect the Ad by encapsulation in a liposome.

Liposome-encapsulated Ad has been investigated for improving transduction in various tumors, especially tumors with negative coxsackievirus and Ad receptor (CAR) expression [22,23,24,25,26]. While previous studies have shown the ability of liposomes to protect Ad from neutralizing antibodies in vitro [27,28], there is little evidence of liposomes protecting Ad in vivo during systemic administration, and few published methods quantitatively assess in vivo protection capabilities of liposomes [29]. Liu et al. is one of the few published studies that explicitly describe an in vivo assay to measure in vivo neutralizing antibody protection of liposome-encapsulated Ad in pre-immunized mouse models [29]. However, this assay relies on liver uptake of the virus and a protocol that measures in vivo antibody neutralization of naked and liposome-protected oncolytic viruses is needed. Inspired by the method described in Liu et al. and blood viral titer measurements, the present study describes a novel method of measuring neutralizing antibody protection. This involves measuring the transduction efficiency of serum isolated from pre-immunized, systemically infected mice. Using the experimental framework in Fig. 2.1, we demonstrate the in vivo protection capabilities of PEGylated DOTAP-folate

liposome-encapsulated Ad (DfAd) and describe the critical components that allow DfAd to protect against neutralizing antibodies.

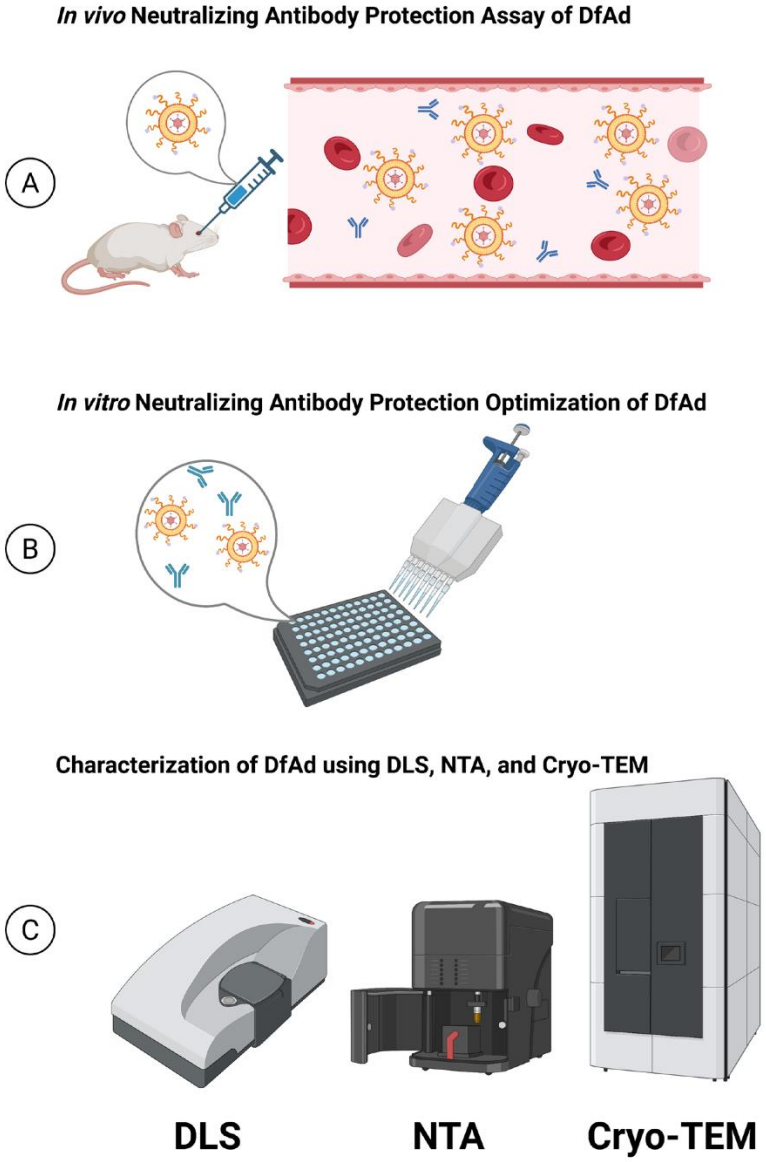

Figure 2.1 Experimental framework for the present study.
The present study is organized around three main experiments. (A) The in vivo neutralizing antibody protection assay was performed on immunized mice to evaluate the in vivo neutralizing antibody protection capabilities of DfAd. (B) The in vitro neutralizing antibody protection assays were performed to optimize the DfAd formulation. (C) DfAd was characterized using dynamic light scattering (DLS), nanoparticle tracking analysis (NTA), and cryogenic transmission electron microscopy (cryo-TEM). Created in BioRender. Phung, A. (2025) https://BioRender.com/31uduc2. Accessed on 26 May 2025.

2.3 Materials and Methods

2.3.1 Reagents and Cell Lines

Replication-deficient Ad expressing green fluorescent protein (Ad-GFP) was purchased from Baylor College of Medicine, Houston, TX, USA (Catalog: Ad5-CMV-eGFP). The HEK293 cell line was purchased from ATCC, Manassas, VA, USA (Catalog: CRL-1573). HEK293 was cultured in complete media of Dulbecco's Modified Eagle Medium (DMEM) with high glucose (Fisher Scientific, Hampton, NH, USA #SH3024301) supplemented with 10% FBS (Omega Scientific, Tarzana, Los Angeles, CA, USA #FB-02) and 1% penicillin–streptomycin–glutamin (PSG, Life Technologies, Carlsbad, CA, USA #10378016).

2.3.2 Synthesis of Liposome-Encapsulated Ad-GFP

Liposome encapsulation of Ad was performed by extrusion, which has been described previously [24]. In brief, DOTAP (Avanti, Alabaster, AL, USA #890890C), cholesterol (Sigma, Saint Louis, MO, USA #C3045), 1,2-distearoyl-sn-glycero-3-phosphoethanolamine-N-[carboxy(polyethylene glycol)-2000] [PEG(2000)-PE carboxylic acid, Avanti #880124P], and 1,2-distearoyl-sn-glycero-3-phosphoethanolamine-N-[folate(polyethylene glycol)-2000] [PEG(2000)-Folate-PE, Avanti #880124P] were mixed together in chloroform at a molar ratio of 1:0.26:0.02:0.01. To make 400 µL of DOTAP-folate Ad-GFP (DfAd-GFP), 387 nmol of DOTAP, 100 nmol of cholesterol, 7.01 nmol of PEG(2000)-PE carboxylic acid, and 3 nmol of PEG(2000)-folate-PE was added to 193.13 µL of chloroform (Sigma, Saint Louis, MO, USA C2432) in an amber vial (Fisher Scientific #03-339-23C). The lipid mixture was vortexed for 30 min at 25 °C. The resulting mixture was vacuumed overnight to form a dry lipid film at the bottom of the vial. The next day, the dry film was rehydrated with 400 µL of phosphate buffered saline (PBS, Fisher Scientific, Hampton, NH, USA #10010072) while vortexing. The hydrated

film was stirred at 600 rpm for 30 min at 4 °C. Empty liposomes were formed by extruding the lipid mixture with the Avanti Mini Extruder (Avanti, Alabaster, AL, USA #6100009-1EA) through a 200 nm membrane (Cytiva/Whatman, UK #10417004), 8 times at room temperature. To the empty liposomes, Ad-GFP was added to reach 5×10^{10} viral particles (vp) mL−1, and the mixture was incubated at room temperature for 30 min to allow for encapsulation of the Ad-GFP. The resulting extruded DfAd-GFP has an Ad to DOTAP lipid ratio [viral particles (VP): nmol] of 5.17×10^{7} [24].

2.3.3 In Vivo Neutralizing Antibody Protection Assay

Six-to-eight-week-old female BALB/c mice were purchased from the Jackson laboratory, Bar Harbor, ME, USA. Mice were housed in high-efficiency particulate air (HEPA) cages in a specific pathogen-free facility with food and water available and a 12 h light/dark cycle. Six mice were immunized with an injected in the right flank with 5×10^{8} viral particles (vp) of unencapsulated Ad (wild-type Ad, Vector Biolabs, Malvern, PA, USA) and another six with an equivalent volume of PBS. Afterwards, the immunized mice developed neutralizing antibodies for at least 21 days. Pain and distress in immunized mice were closely monitored. After a minimum of 21 days, six mice (three immunized with Ad and three immunized with PBS) were retro-orbitally (RO) injected with 5×10^{9} vp of DfAd-GFP and the other six with Ad-GFP under isoflurane sedation. The injected orbital sinus was immediately anesthetized with 0.5% proparacaine hydrochloride ophthalmic drops (Sigma Pharmaceuticals, North Liberty, IA, USA #4503-2). Pain and distress in the RO-injected mice were closely monitored. After waiting 5 min, mice were sacrificed, and blood was collected from each mouse using cardiac puncture. All procedures and protocols were approved by the UC San Diego Institutional Animal Care and Use Committee (IACUC).

Serum was isolated from each mouse blood sample by leaving the blood to coagulate in an Eppendorf tube on ice for 30 min. Each blood sample was centrifuged at 400× g for 5 min at 4 °C, and the top layer of serum was collected. HEK293 cells plated at 3×10^4 cells per well in 96-well plates were then transduced with 50 µL of each serum sample (day 1). The cells were then incubated at 37 °C at 5% CO2 for 24 h. GFP fluorescence intensities were measured using a Tecan F PLEX Infinite 200 Pro microplate reader on day 2.

2.3.4 Fluorescence Microscopy

Cells transduced with DfAd-GFP or Ad-GFP were analyzed under a Keyance BZ-X710 microscope (KEYENCE CORPORATION OF AMERICA, Itasca, IL, USA) with a GFP filter and 470/40 nm excitation wavelength, 525/50 nm emission wavelength and dichroic mirror wavelength of 495 nm. Comparative micrographs were captured using 2× and 20× objective lenses. Cell counting was performed using images taken with the 20× objective lens.

2.3.5 In Vitro Neutralizing Antibody Protection Assay

HEK293 cells were plated at between 1×10^4 to 3×10^4 cells well−1 in 96-well plates and incubated at 37 °C and 5% CO2 in complete media. A neutralizing antibody protection assay was performed after cells were attached to the well (24–48 h after plating). Media in the wells was removed from the wells without disturbing the cells. DfAd-GFP or Ad-GFP was mixed with 1/10× serum (human or mouse) and added to the cells at MOI 100 with enough volume to cover the cells (day 1). Cells were then incubated at 37 °C and 5% CO2 for 1 h before the mixture was removed from the wells and replaced with fresh complete media, trying not to disturb the cells. The cells were incubated again at 37 °C and 5% CO2 for 24 h. GFP fluorescence intensities were measured using a Tecan F PLEX Infinite 200 Pro microplate reader (Tecan Group Ltd., Männedorf, Switzerland) on day 2.

2.3.6 Cryo-Transmission Electron Microscopy (Cryo-TEM)

Quantifoil carbon R2/2 copper grids were acquired from Quantifoil Micro Tools GmbH (Jena, Germany). Cryo-TEM imaging was performed using a JEOL JEM-2100F transmission microscope (JEOL USA, Peabody, MA, USA). Before imaging, grids were glow discharged using a Solarus Plasma Cleaner 950 (Gatan, Inc., Pleasanton, CA, USA). An amount of 3 µL of each sample was applied to a grid before sample freezing. Blotting and freezing were performed at room temperature and 95% humidity using a Leica EMGP plunger (Leica Microsystems Inc., Deerfield, IL, USA). Blotting time was set to 3 s without waiting or draining steps. Frozen grids were loaded on a cold Gatan cryo-transfer holder (Gatan, Inc., Pleasanton, CA, USA) and imaged at 30,000× magnification. Images were captured on a Gatan OneView CCD (Gatan, Inc., Pleasanton, CA, USA) with SerialEM software 4.2.0 (University of Colorado, Boulder, CO, USA). Images were processed using Fiji 2.16.0/1.54p.

2.3.7 Statistical Analysis

Prism 10.4.1 software (GraphPad Software LLC, Boston, MA, USA) was used for data analysis. Comparison between the two groups was based on a two-tailed unpaired t-test. A value of $p < 0.05$ was determined to be statistically significant.

2.4 Results

2.4.1 In Vivo Neutralizing Antibody Protection Assay

Fig. 2.2A shows the mouse immunization and injection schedule for the in vivo neutralizing antibody protection assay, which will measure the protection by the liposomal coating against neutralizing anti-Ad antibodies in circulation inside of immunized mice. After mice were immunized with Ad for 21 days, they were systemically administered DfAd-GFP or Ad-GFP, which were allowed to circulate for 5 min before the mice were sacrificed and their

blood was collected. Five minutes of circulation time equates to at least 20 passes through the mouse circulatory system and provides sufficient exposure time to neutralizing antibodies with minimal involvement of liver and macrophage clearance systems [30,31]. The number of viable viruses in the blood was assessed by transfecting HEK293 cells with isolated serum infected with DfAd-GFP or Ad-GFP and fluorescence was read using a Tecan fluorescent plate reader.

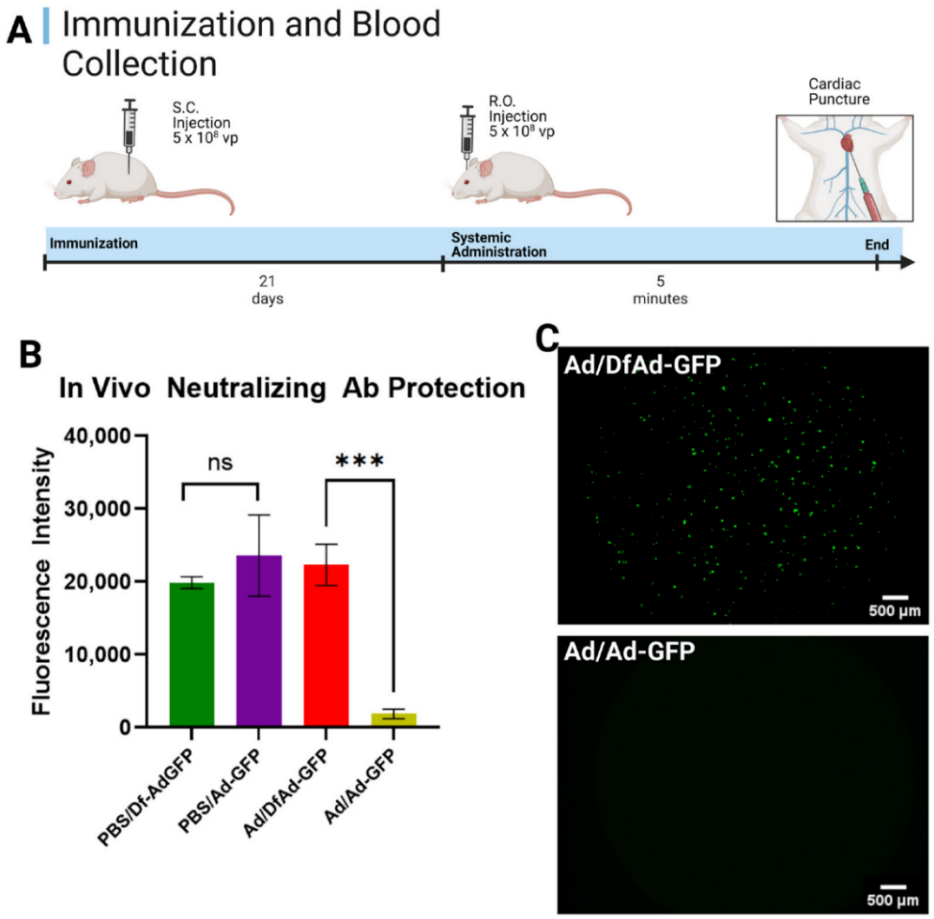

Figure 2.2 In vivo neutralizing antibody protection of DfA against pre-existing anti-Ad antibodies.
(A) Schedule for mouse immunization, sample administration, and cardiac puncture. Immunocompetent Balb/c mice are immunized subcutaneously with 5×10^8 vp of Ad or an equal volume of PBS. Twenty-one days later, mice are RO-treated with 5×10^8 vp DfAd-GFP or Ad-GFP; 5 min later, mice are sacrificed, and blood is collected via cardiac puncture. (B) In vivo neutralizing antibody protection assay performed by transducing HEK293 cells with serum from PBS or Ad-immunized mice systemically treated with either Df-AdGFP or Ad-GFP. PBS/DfAd-GFP = transduction efficiency of serum extracted from mice immunized with PBS and systemically injected with DfAd-GFP (green). PBS/Ad-GFP = transduction efficiency of serum extracted from mice immunized with PBS and systemically injected with Ad-GFP (purple). Ad/DfAd-GFP = transduction efficiency of serum extracted from mice immunized with Ad and systemically injected with DfAd-GFP (red). Ad/Ad-GFP = transduction efficiency of serum extracted from mice immunized with Ad and systemically injected with Ad-GFP (gold). *** $p < 0.001$, $n = 4$. (C) Fluorescent micrographs of HEK293 cells transduced with serum from a mouse immunized with Ad and systemically injected with Df-AdGFP (top) and a mouse immunized with Ad and systemically injected with Ad-GFP (bottom). Both images were auto leveled using the preview application to improve contrast. Created in BioRender. Phung, A. (2025) https://BioRender.com/4eh0ucc. Accessed on 26 May 2025.

Fig. 2.2B shows the results of the in vivo neutralizing antibody assay on mice immunized by PBS and systemically injected with DfAd-GFP (the green bar, PBS/Df-Ad-GFP); immunized by PBS and systemically injected with Ad-GFP (the purple bar, PBS/Ad-GFP); immunized by Ad and systemically injected with DfAd-GFP (the red bar, Ad/DF-Ad-GFP); and immunized by Ad and systemically injected with Ad-GFP (gold bar, Ad/Ad-GFP). The assay shows that the serum of mice that were immunized with PBS showed no difference in transduction efficiency in HEK293 cells, whether they were systemically injected with DfAd (green) or Ad (purple). This result confirms that mice were consistently injected with the same number of viral particles and that other Ad clearance systems were minimally involved. However, when mice were immunized with Ad, serum from mice that were systemically injected with DfAd-GFP (red, Ad/DF-Ad-GFP) demonstrated 12× higher transduction efficiency compared with serum of mice that were injected with unencapsulated Ad-GFP (gold, Ad/Ad-GFP). This result shows that DfAd-GFP was protected from circulating neutralizing antibodies in immunized mice and that more viable DfAd-GFP were recovered in serum compared with unencapsulated Ad-GFP. Significantly fewer Ad-GFP were recovered in serum without liposome protection in vivo, resulting in 12× lower transduction efficiency. Fig. 2.2C shows fluorescent micrographs of wells containing HEK293 cells that were treated with serum from a mouse that was Ad-immunized and RO-injected with DfAd-GFP (top image) and cells that were treated with serum from a mouse that was Ad-immunized and RO-injected with unencapsulated Ad-GFP. The top image demonstrates significantly more fluorescent HEK293 compared with the bottom image, which shows no fluorescent HEK293 cells.

2.4.2 In Vitro Optimization of DfAd for Protection Against Neutralizing Antibodies

The formulation of DfAd, cholesterol concentration, PEG lipid concentration, folate PEG lipid concentration, and PEG lipid length were adjusted to determine the critical components that provide DfAd protection against neutralizing antibodies in vitro. Experiments in Fig. 2.3A,B used 10× diluted neutralizing serum from immunized mice so that there would be repeatable results between serum batches. Figure 2.3A shows the results of optimizing the cholesterol concentration in DfAd, where changing the concentration of cholesterol by 50% did not affect the protection against neutralizing antibodies, as evidenced by the marginal change in transduction efficiency in 1/10× mouse serum. Altogether omitting cholesterol from the DfAd formulation lowered the protection by ~50%. In Fig. 2.3B, results show that removing DSPE-PEG2000-folate, the cancer-targeting lipid PEG peptide, from the DfAd formulation did not affect the protection against neutralizing antibodies. However, removing DSPE-PEG2000-CA (typically used to stabilize liposomes in aqueous solution) reduced protection by ~70%.

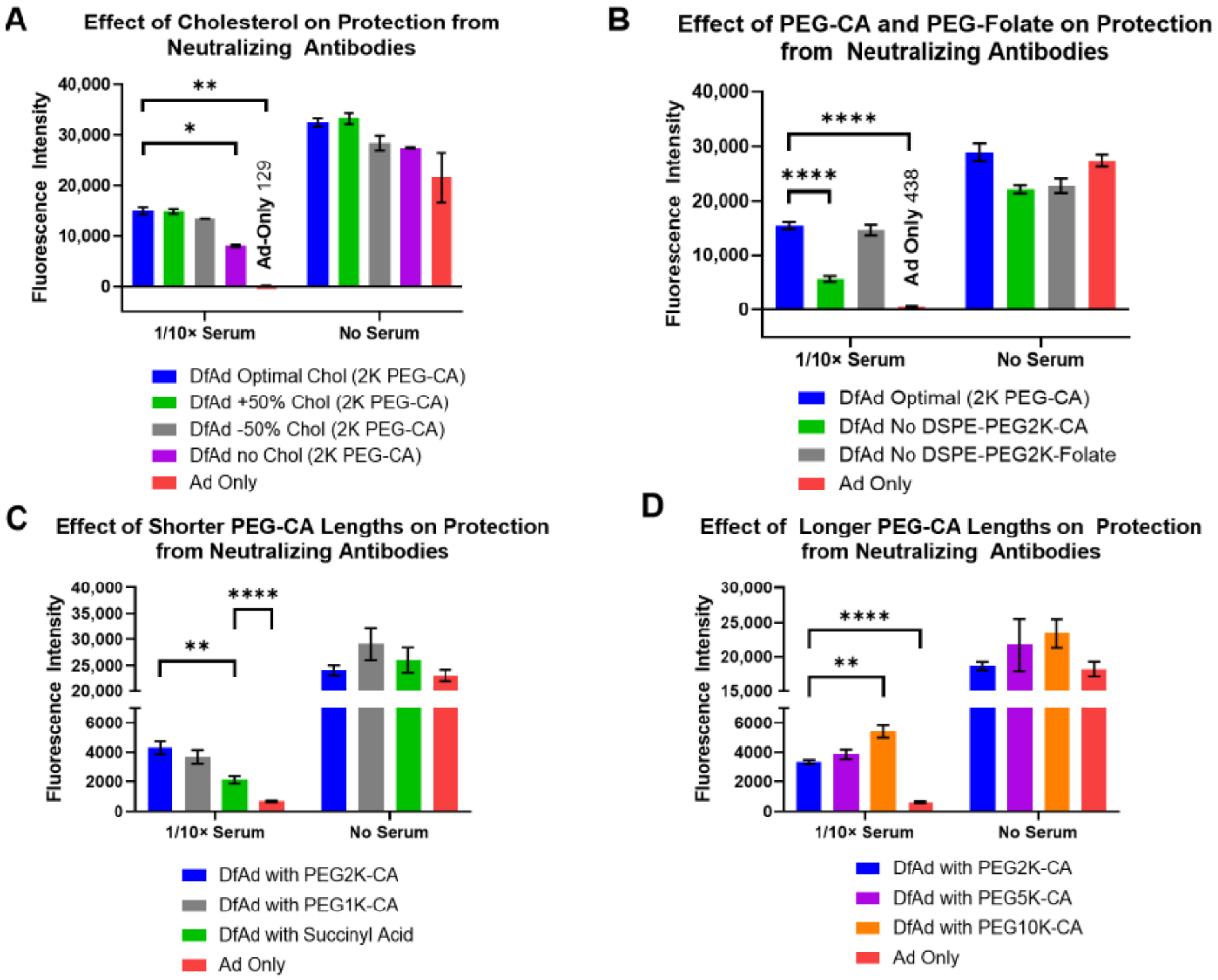

Figure 2.3 Effect of liposome formulation on in vitro protection from neutralizing antibodies.
(A) The effect of cholesterol composition on liposomal protection from neutralizing antibodies. This experiment used neutralizing serum from immunized mice. * $p \leq 0.05$, ** $p \leq 0.01$, $n = 2$. (B) The effect of incorporating PEG2000-CA and PEG2000-Folate on liposomal protection from neutralizing antibodies. This experiment used neutralizing serum from immunized mice. **** $p \leq 0.0001$, $n = 4$. (C) The effect of incorporating shorter PEG lipids on liposomal protection from neutralizing antibodies. This experiment used neutralizing serum from human blood samples. ** $p \leq 0.01$, **** $p \leq 0.0001$, $n = 6$. (D) The effect of incorporating longer PEG lipids on liposomal protection from neutralizing antibodies. This experiment used neutralizing serum from human blood samples. ** $p \leq 0.01$, **** $p \leq 0.0001$, $n = 6$.

Experiments shown in Fig. 2.3C,D used neutralizing serum from human blood samples to benchmark the protective capabilities of DfAd in serum with clinically relevant neutralizing antibody titers. The results show that replacing the DSPE-PEG2000-CA in the DfAd formulation

with DSPE-PEG5000-CA or with DSPE-PEG1000-CA barely changed the protection against neutralizing antibodies. However, by replacing DSPE-PEG2000-CA with DSPE-succinyl acid (DSPE-CA, no PEG chain) or DSPE-PEG10k-CA, protection against neutralizing antibodies was lowered by ~50% or increased by about ~60%, respectively. The latter results suggest that extremely long PEG enhances protection against neutralizing antibodies.

2.4.3 Characterization of DfAd

Physical characterization was performed using the optimized formulation with single variations to determine the correlation between in-vitro neutralizing antibody protection and physical stability. Dynamic light scattering (DLS), nanoparticle tracking analysis (NTA), and transmission electron microscopy (TEM) were used to measure the size and assess the structural stability of DfAd.

As shown in Table 2.1 and Fig. 2.4, DLS size measurements showed that the optimal DfAd with DSPE-PEG2K-CA was ~206 nm, with a uniform polydispersity index of 0.15. Note that all measurements in Table 1 are taken without stirring. Replacing the DSPE-PEG2000-CA with DSPE-PEG10K-CA in the DfAd formulation increased the DfAd hydrodynamic size to ~215 nm, while maintaining a uniform polydispersity of 0.18. However, by replacing DSPE-PEG2000-CA with DSPE-PEG1000-CA, the size of DfAd increased very slightly to ~514 nm, with an increased polydispersity index of 0.59. Completely removing DSPE-PEG2000-CA further increases the size of DfAd to ~3870 nm with an increased polydispersity index of 0.68. Figure 2.4A,B show graphical descriptions of the data in Table 2.1. They visually demonstrate the changes in size and dispersity between the DfAd with DSPE-PEG2K-CA and no DSPE-PEG-CA, where size increases by 19 fold, and dispersity increases 5 fold. The increased size and polydispersity with the removal of DSPE-PEG are consistent with the loss of physical stability of

the DfAd, resulting in aggregation or flocculation of the nanoparticles. DfAd sizes were again measured using nanoparticle tracking analysis (NTA) to confirm these observations.

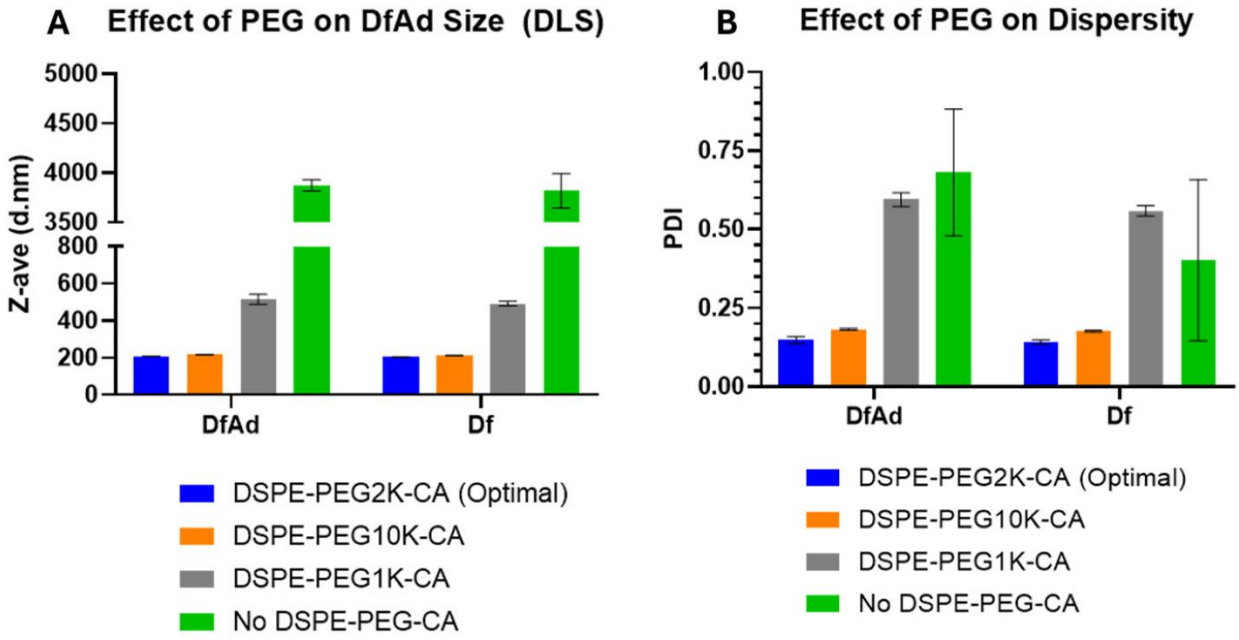

Figure 2.4 Characterization of various DfAd formulations using DLS.
(Table 2.1) The effect of PEG lipid composition and length on the particle size using DLS on DfAd. Fold change refers to the relative change in z-average diameter or PDI of the DfAd sample of interest compared with the z-average diameter or PDI of DfAd with DSPE-PEG2000-CA. (A) Graphical representation of the effect of PEG on DfAd size. (B) Graphical representation of the effect of PEG on particle dispersity (uniformity).

Table 2.1: The effect of PEG Lipid composition and length on particle size using DLS of DfAd (n = 3). SEM is the standard error of the mean of n=3 different runs, not the distribution of the nanoparticle size.

Sample	z-Average (nm)	Fold Change (z-Average)	Polydispersity Index (PDI)	Fold Change (PI)
DfAd DSPE-PEG2K-CA	206 ± 2	1	0.1 ± 0.0	1
Df DSPE-PEG2K-CA (Empty Liposomes)	203 ± 2	1	0.1 ± 0.0	1
DfAd No DSPE-PEG-CA	3870 ± 57	19	0.7 ± 0.2	5
Df No DSPE-PEG-CA (Empty Liposomes)	3820 ± 175	19	0.4 ± 0.3	3
DfAd DSPE-PEG1K-CA	515 ± 27	3	0.6 ± 0.0	4
Df DSPE-PEG1K-CA (Empty Liposomes)	492 ± 12	2	0.6 ± 0.0	4
DfAd DSPE-PEG10K-CA	216 ± 1	1	0.2 ± 0.0	1
Df DSPE-PEG10K-CA (Empty Liposomes)	211 ± 2	1	0.2 ± 0.0	1

NTA measurements in Table 2.2 and Figure 2.5 were taken of each sample without a stirring step between each read. With the removal of the stirring in between each read, the DfAd size was 136 nm. However, the DfAd without DSPE-PEG2000-CA increased by more than 2×, reaching 291 nm in diameter. Fig. 2.5A,B show the particle size distributions of DfAd using DSPE-PEG2K-CA and no DSPE-PEG-CA, respectively, with a uniform distribution in Fig. 2.5A and a more polydisperse distribution in Fig. 2.5B. Increasing nanoparticle size with the removal of DSPE-PEG is consistent with flocculation, similar to the DLS experiment in Figure 2.4.

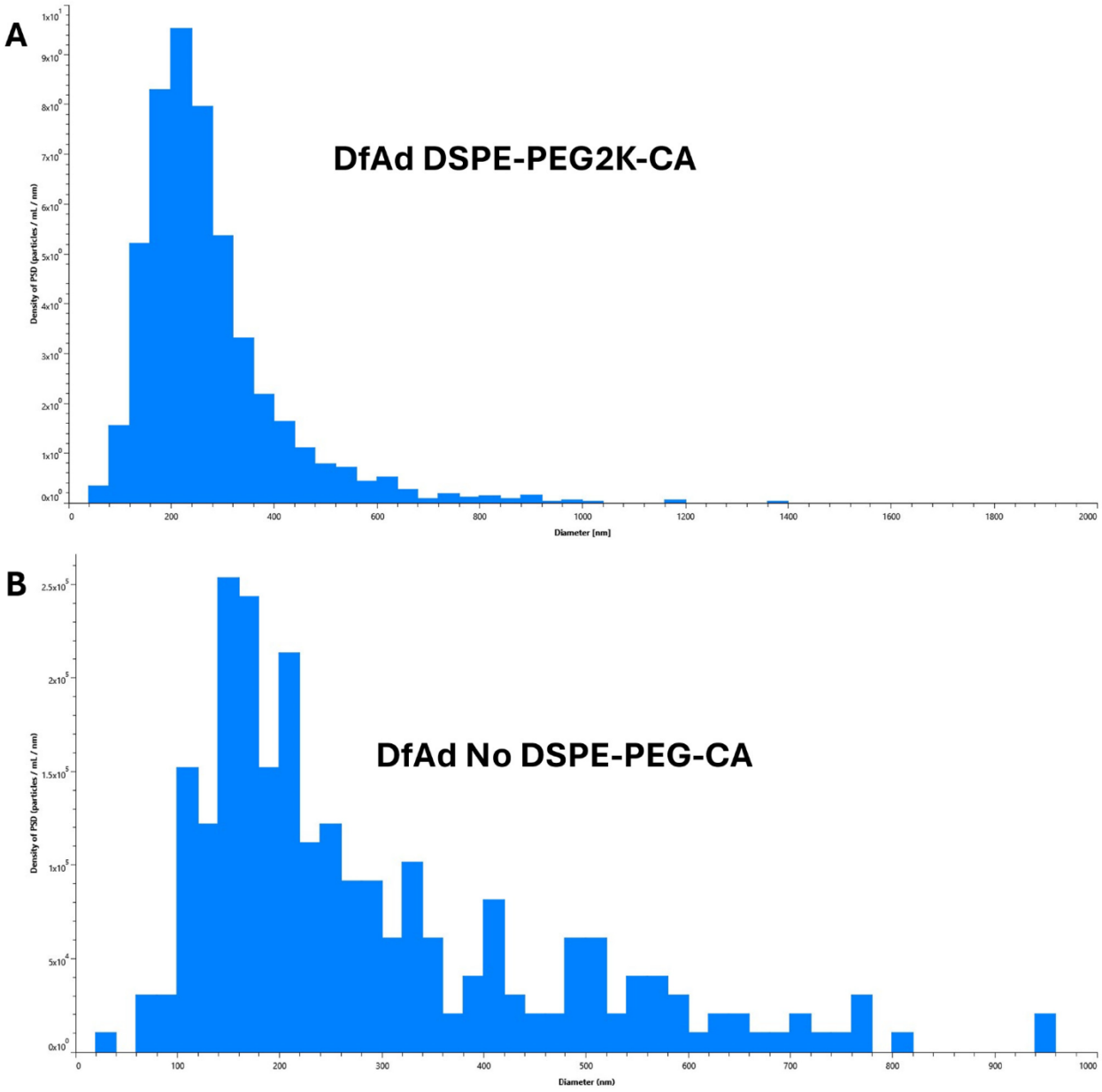

Figure 2.5 Characterization of various DfAd formulations using NTA without stirring. (Table 2.2) The effect of PEG lipid composition and length on particle size using NTA on DfAd without stirring. Fold change refers to the relative change in mean diameter of the DfAd sample of interest compared with the average diameter of DfAd with DSPE-PEG2000-CA. (A) Graphical size distribution of DfAd particles formulated with DSPE-PEG2K-CA. (B) Graphical size distribution of DfAd particles formulated without DSPE-PEG-CA.

Table 2.2 The effect of PEG Lipid composition and length on particle size of DfAd using NTA (Without Stirring).

Sample	Mean Diameter (nm)	Fold Change (Diameter)	D10, D50, D90 (nm)
DfAd DSPE-PEG2K-CA	136	1.0	73, 120, 215
DfAd No DSPE-PEG-CA	291	2.1	127, 230, 560

NTA measurements shown in Table 2.3 and Fig. 2.6 were first performed by stirring at 1400 RPM for 3 s between each read. NTA measurements showed that DfAd had a mean size of 145 nm. Replacing the DSPE-PEG2000-CA with DSPE-PEG1000-CA changed the size slightly to 128 nm, and replacing it with DSPE-PEG5000-CA changed the size slightly to 165 nm. Removing the DSPE-PEG2000-CA changed the size slightly to 134 nm. All four mean diameters are generally very similar, where all sizes are within ±10% of the DfAd DSPE-PEG2000-CA mean diameter. Fig. 2.6A–D show the particle size distributions of DfAd using DSPE-PEG2K-CA, no DSPE-PEG-CA, DSPE-PEG1K-CA, and DSPE-PEG5K-CA, respectively, demonstrating uniform size distributions in all four samples. Fig. 2.6A,B demonstrate very similar distributions, with their peaks hovering over ~120 nm. In Fig. 2.6C, the curve is shifted very slightly to the left with the peak hovering over ~100 nm, and in Fig. 2.6D is shifted very slightly to the right with the peak hovering over ~140 nm. Stirring between NTA reads likely breaks up flocculated nanoparticles and reestablishes uniformity in DfAd nanoparticle sizes, especially for the DfAd without DSPE-PEG-CA. The DfAd with DSPE-PEG2000-CA remains the same size with and without stirring, likely due to PEG preventing flocculation of the particles. NTA experiments demonstrate consistent observations made during DLS experiments, where DSPE-PEG2000-CA helps form smaller, more uniform nanoparticles while the removal of DSPE-PEG2000-CA forms larger, more polydisperse ones.

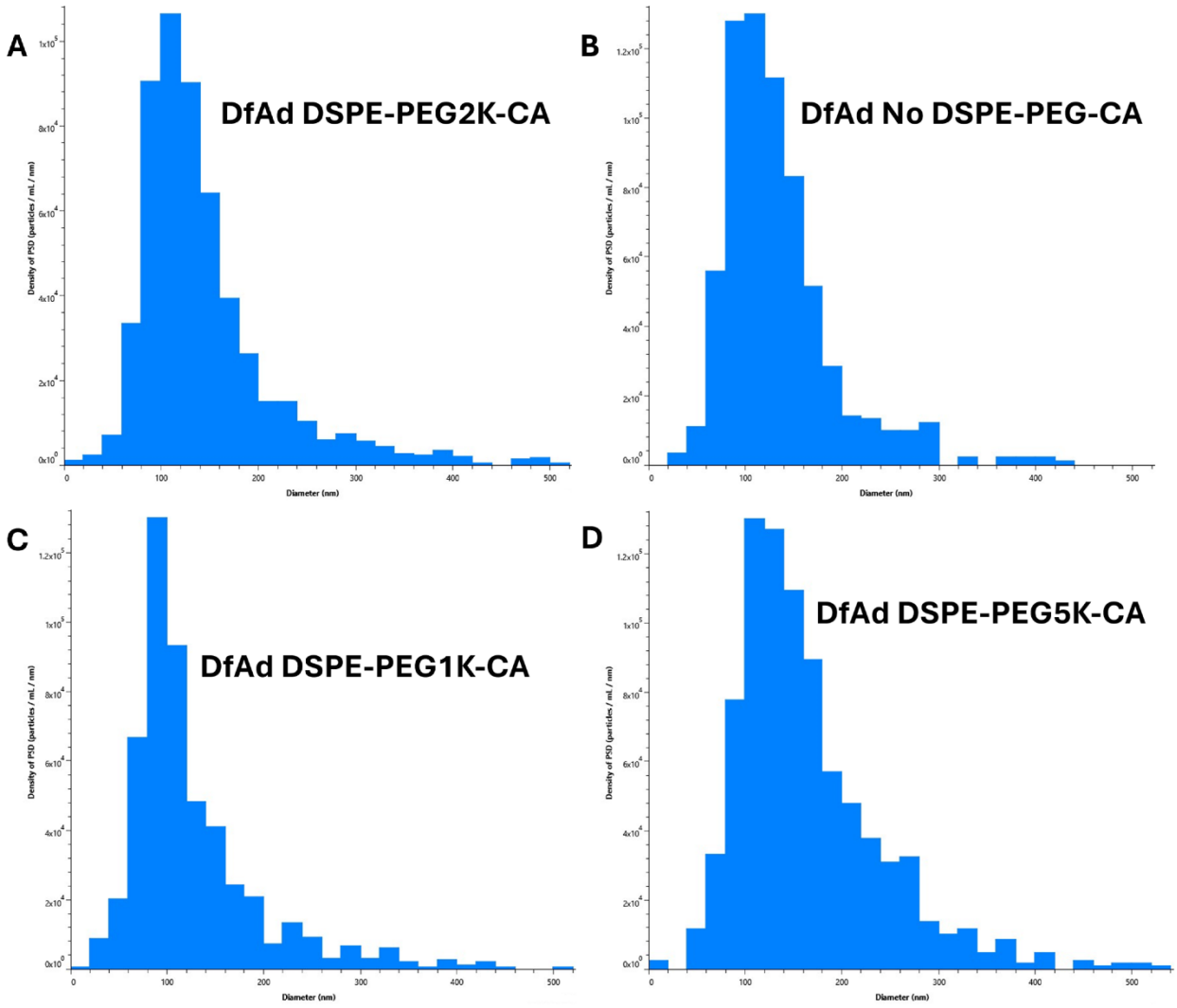

Figure 2.6 Characterization of various DfAd formulations using NTA with stirring. (Table 2.3) The effect of PEG lipid composition and length on particle size using NTA on DfAd with stirring. Fold change refers to the relative change in mean diameter of the DfAd sample of interest compared with the average diameter of DfAd with DSPE-PEG2000-CA. (A) Graphical size distribution of DfAd particles formulated with DSPE-PEG2K-CA. (B) Graphical size distribution of DfAd particles formulated without DSPE-PEG-CA. (C) Graphical size distribution of DfAd particles formulated with DSPE-PEG1K-CA. (D) Graphical size distribution of DfAd particles formulated with DSPE-PEG5K-CA.

Table 2.3 The effect of PEG Lipid composition and length on particle size of DfAd using NTA (With Stirring).

Sample	Mean Diameter (nm)	Fold Change (Diameter)	D10, D50, D90 (nm)
DfAd DSPE-PEG2K-CA	145	1.0	82, 125, 234
DfAd No DSPE-PEG-CA	134	0.9	79, 121, 202
DfAd DSPE-PEG1K-CA	128	0.9	68, 105, 223
DfAd DSPE-PEG5K-CA	165	1.1	90, 148, 264

The cryo-TEM images in Fig. 2.7 show that the Ad and the liposome coating can be distinguished. In Fig. 2.7A,B, the liposome encapsulation appears to be of thin dark layers around darkened spheres of 70–80 nm in diameter. The diameter of the encapsulated dark spheres is around 80–90 nm. Fig. 2.7A shows two separated DfAd nanoparticles marked with green arrows. Fig. 2.7B shows eight DfAd nanoparticles bunched together, each marked with a green arrow. Liposome-encapsulated adenovirus in both Fig. 2.7A,B are tightly enveloped with about 5–10 nm of space separating the surface of the virus from the lipid bilayer. While removing DSPE-PEG2000-CA did not change the size of the encapsulated virus, the DfAd without DSPE-PEG-CA appeared more bunched together, and the liposomes appeared to be more hexagonal than spherical, compared with the DfAd with DSPE-PEG2000-CA. In Fig. 2.7C, the viruses are shown to be darkened spheres of roughly 70–80 nm in diameter. Five viral particles are each marked with green arrows. In Supp. Fig. 2.4A, there are two DfAd that are encapsulated together in one larger liposome. Supp. Fig. 2.4B shows DfAd without DSPE-PEG-CA, with similar shaped liposomes as in Fig. 2.7B, except that the nanoparticles in Supp. Fig. 4B are less bunched together.

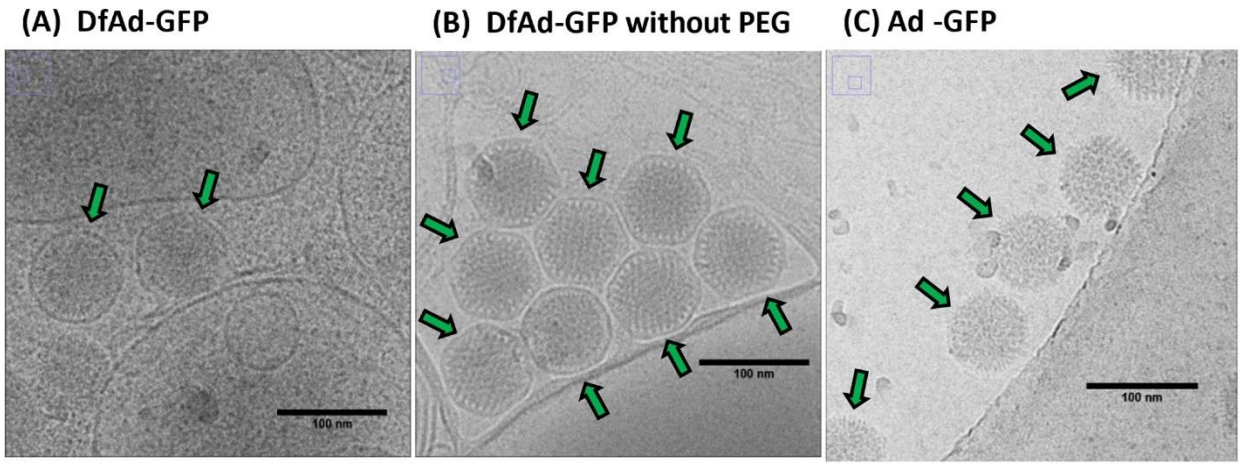

Figure 2.7 Characterization and structural analysis of DfAd.
(A) Cryo-TEM image of DfAd-GFP at 30,000× magnification plus a 50% digital zoom. Green arrows point to liposome-encapsulated Ad-GFP. (B) Cryo-TEM image of DfAd-GFP without PEG at 30,000× magnification plus a 50% digital zoom. Green arrows point to liposome-encapsulated Ad-GFP without PEG. (C) Cryo-TEM image of Ad-GFP without encapsulation at 30,000× magnification plus a 50% digital zoom. Green arrows point to naked, unencapsulated Ad-GFP. In all figures, the scale bar for cryo-TEM images is 100 nm.

2.5 Discussion

The present study demonstrates the in vivo protection of DfAd against neutralizing antibodies by directly exposing DfAd as well as unencapsulated Ad to circulating neutralizing antibodies and evaluating the viable virion after five minutes of circulation. Most of the DfAd remained un-neutralized during five minutes of circulation time in pre-immunized mice, while unencapsulated Ad were almost completely neutralized during the same circulation time. A five-minute circulation time equates to roughly 20 complete passes through a mouse's blood system, assuming one pass is 15 s [31]. Fig. 2.8A summarizes how DfAd is protected from pre-existing neutralizing antibodies, allowing for prolonged circulation while retaining most of its activity when compared with unencapsulated Ad, which becomes neutralized immediately when exposed to pre-existing antibodies and loses almost all activity. Previous studies encapsulating Ad with liposomes have also shown in vivo neutralizing antibody protection with similar platforms [29].

However, these studies evaluated in vivo protection by measuring liver cell transduction efficiency in immunized mouse models. While liver transduction could be an accurate method of evaluating in vivo neutralizing antibody protection, a more direct method is needed. The liver transduction method theoretically suggests that increased transduction of liver cells by encapsulated Ad in pre-immunized mice translates to increased protection. Because liver uptake of therapeutic viruses and nanoparticles is usually discouraged as it removes the therapeutic from systemic circulation (except for the case of treating liver cancers) [32,33,34,35,36,37], there is a need for other methods of assessment. Measuring the activity of viable encapsulated Ad in the blood after circulation is a more direct method to evaluate in vivo protection against neutralizing antibodies as a model for the potential therapeutic efficacy of encapsulated and unencapsulated oncolytic Ad neutralizing environment. To directly measure the viable encapsulated or unencapsulated Ad in the blood, pre-immunized Balb/c mice were systemically administered Ad engineered with the GFP transgene, allowing measurement of GFP fluorescence in HEK293 cells transfected with the infected mouse serum and evaluate protection against neutralizing antibodies by measuring the transduction efficiency of each serum sample. A schematic of the entire protocol is shown in Supp. Fig. 2.1. Using Ad-GFP instead of Ad-β-gal, as undertaken by Yotnda et al. and Liu et al., for in vitro and in vivo neutralizing assays, allows for quicker assay time and removes the need to fix and stain cells and tissues [27,29]. By measuring the transduction efficiency of the isolated serum samples directly, the present study's assay more accurately evaluates the protective capabilities of the liposome coating compared with liver transduction measurements in previous literature.

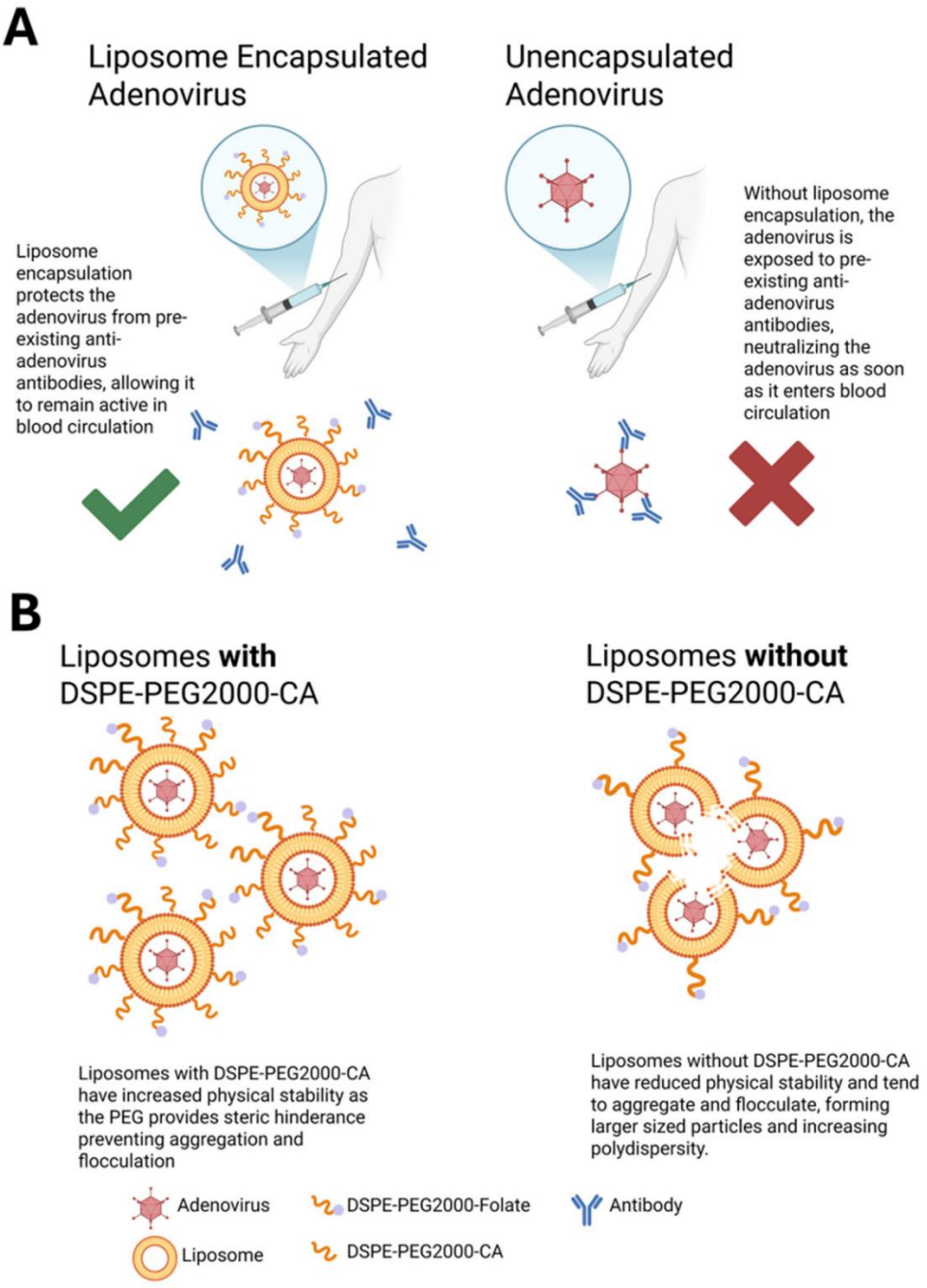

Figure 2.8 Summary schematic of PEGylated liposome-encapsulated Ad.
(A) Schematic of liposome protecting encapsulated Ad from neutralizing antibodies in circulation. Without encapsulation, Ad is exposed to surrounding neutralizing antibodies in the blood and is immediately neutralized. (B) Schematic of DSPE-PEG2000-CA's role in increasing stability of DfAd, resulting in smaller, more uniform nanoparticles. Removal of DSPE-PEG2000-CA results in reduced stability, causing aggregation between nanoparticles and increasing their size. (A) was created in BioRender. Phung, A. (2025) https://BioRender.com/hs8e533. Accessed on 26 May 2025. (B) was also created in BioRender. Phung, A. (2025) https://BioRender.com/j53c141. Accessed on 26 May 2025.

Liposome encapsulation is a viable method for protecting Ad from neutralizing antibodies when administering oncolytic Ad vectors systemically. Encapsulation of adenovirus was confirmed using cryo-TEM qualitatively, shown in Fig. 2.7. Encapsulation rate was quantitatively measured at 96% by manually counting liposomes in cryo-TEM images, shown in Supp. Fig. 2.2 [24]. One possible mechanism of encapsulation is surface-tension-induced self-assembly, which suggests negatively charged adenoviruses are spontaneously encapsulated by small, empty cationic liposomes via self-assembly, thereby forming DfAd [24]. Hypothetically, the high surface tension of the small liposomes, and the charge interactions between the cationic liposome and the negatively charged adenovirus, drive the spontaneous encapsulation as shown in Supp. Fig. 2.3 [24,38]. Cryo-TEM images show partially encapsulated adenovirus, which suggest that viral particles can penetrate the lipid membrane to form DfAd [24]. Similar to the present study, previous studies using liposome encapsulation of Ad have demonstrated increased transduction efficiency in the presence of neutralizing serum in vitro when compared with unencapsulated Ad [27,28]. However, the present study reveals a novel correlation between liposome stability and neutralizing antibody protection by first quantifying the critical components of DfAd that affect protection against neutralizing antibodies of the encapsulating liposome. The optimization experiments in the present study demonstrate that DSPE-PEG2000-CA and cholesterol are critical components of DfAd that protect the Ad from neutralizing antibodies, as evidenced by significant reduction to the neutralizing antibody protection when removing either component from the DfAd formulation. Experiments also showed that PEG length correlates with neutralizing antibody protection, where DfAd with DSPE-succinyl acid provided the least protection against neutralizing antibodies while DfAd with DSPE-PEG10K-CA provided the most protection against neutralizing antibodies. To further investigate how

these critical components affect DfAd, DLS, NTA, and Cryo-EM characterizations were used to measure the physical stability and morphology of DfAd when these components are removed.

Characterization of DfAd by DLS suggests that the nanoparticles become unstable at room temperature without DSPE-PEG2000-CA, manifested by significant increases in size and polydispersity index. Evidence from the NTA measurements without stirring shows that a similar observation is made between DfAd with and without DSPE-PEG2000-CA, where the size almost doubles without the PEG stabilizing the nanoparticles. Although cryo-EM images also show that the sizes of DfAd and DfAd without PEG do not change significantly, the sample without DSPE-PEG2000-CA appears more bunched together than DfAd with PEG. PEG is usually added to liposomes to increase stability and prevent flocculation and sedimentation, as it provides a physical barrier blocking other biomolecules and other liposomes from them [39,40,41]. Removing DSPE-PEG2000-CA from the formulation removes this barrier, causing them to bunch together, aggregate, and fuse, forming larger, more polydisperse nanoparticles, as observed from characterization experiments.

A similar aggregation effect is observed in DfAd when the PEG length is shortened significantly, as DLS showed by incorporating DSPE-PEG1000-CA, where the liposomes already start to grow and lose uniformity. This suggests that, by shortening the PEG chain below 2000 Daltons, the liposomes will destabilize and aggregate. Although this was not confirmed with NTA or cryo-EM, previous studies have shown that longer PEGs generally provide more physical stability for liposomes when compared with shorter PEGs, as they form a denser steric barrier from surrounding liposomes and biomolecules [42,43]. Lengthening PEG molecules on the surface of nanoparticles, however, is also shown to reduce their cellular uptake via the same steric hindrance mechanism that prevents nanoparticle agglomeration [44]. Therefore, PEG

length selection is a balancing act between many different factors to improve delivery [45]. Therefore, although DSPE-PEG10K-CA demonstrated better protection against neutralizing antibodies compared with DSPE-PEG2K-CA, further studies are needed to determine whether PEG10K or PEG2K is better.

Fig. 2.8B summarizes how PEG prevents aggregation between DfAd while removal results in aggregation between DfAd nanoparticles. The correlations between PEG concentration and in vitro antibody protection, as well as PEG length and in vitro antibody protection, bring to attention a potential direct link between physical stability and neutralizing antibody protection, one which requires further study. Previous studies have shown liposome aggregation and the membrane fusion that is due to poor stability can cause liposomes to become "leaky," allowing encapsulated small molecule cargo to escape [46,47,48,49]. The "leaky" liposome theory could be a potential mechanism by which neutralizing antibodies bypass liposomes lacking PEG or grafted with short PEGs, motivating further investigation.

2.6 Conclusions

The present study demonstrates a novel method of evaluating neutralizing antibody protection by liposome-encapsulated Ad in immunized mouse models. By systemically injecting DfAd-GFP into preimmunized mice, extracting the blood, and transfecting HEK293 reporter cells with the infected serum, the in vivo neutralizing antibody protection assay assesses the protective capabilities of the DfAd-GFP liposome by measuring the fluorescence emitted from the transduced HEK293 cells. Based on the in vivo neutralizing antibody protection experiment results, DfAd can circulate in the blood without being neutralized for at least 5 min, allowing ~20 passes throughout the mouse body. The study also combined in vitro neutralizing antibody assays and characterization data to reveal a unique correlation between the structural stability of

the liposome and neutralizing antibody protection by identifying DSPE-PEG and cholesterol as critical components for neutralizing antibody protection. The optimized DfAd is a viable platform to protect encapsulated Ad from neutralizing antibodies as it not only protects against neutralizing antibodies in diluted serum but protects against neutralizing antibodies in circulation in immunized mouse models. The results of this study provide novel methodologies and design insights for the clinical translation of systemic oncolytic viral therapy.

2.7 Acknowledgements

Chapter 2, in full, is a reprint of the material as it appears in Pharmaceutics 2025. Phung, Abraham T.; Shah, Jaimin R.; Dong, Tao; Aisagbonhi, Omonigho; Trogler, William C.; Kummel, Andrew C.; Blair, Sarah L. MDPI, 2025. The dissertation author was the primary author of this paper.

2.8 Supplementary Material

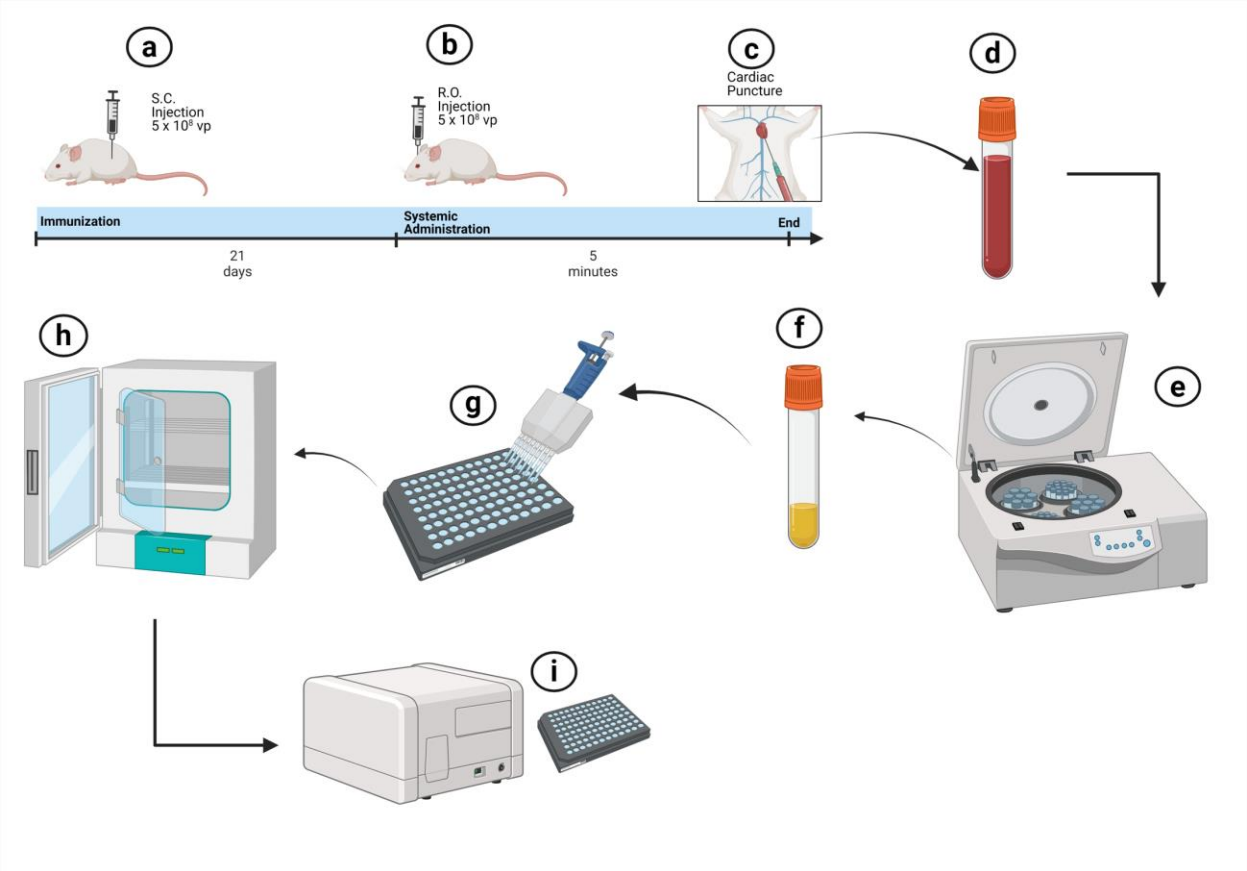

Supplementary Figure 2.1 Schematic of the In Vivo Neutralizing Antibody Protection Assay.
Figure shows an overview of the different steps of the in vivo neutralizing antibody assay described in Figure 4. (a) Balb/c mice are immunized for 21 days with one subcutaneous injection of Ad or PBS. (b) Mice are injected retro-orbitally with Ad-GFP or DfAd-GFP, which are allowed to circulate for five minutes. (c) Blood is extracted from mice by cardiac puncture and transferred to (d) heparin blood collection tubes. (e) Blood is transferred to Eppendorf tubes, incubated on ice for 30 minutes, and centrifuged at 3,000 RPM for 10 minutes. (f) The resulting serum is isolated into separate tubes on ice. (g) HEK293 cells pre-plated 24 hours earlier are treated with the resulting serum and (h) incubated at 37℃ for 24-48 hours. (i) The resulting fluorescence was measured using a fluorescence plate reader. Created in BioRender. Phung, A. (2025) https://BioRender.com/k19q694. Accessed 26 May 2015.

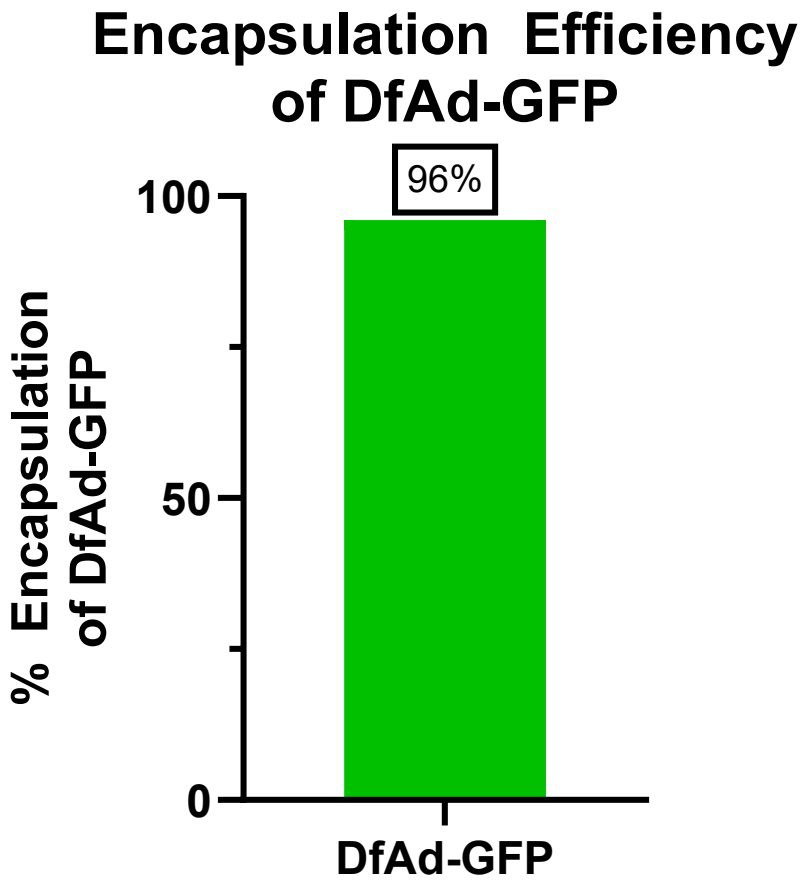

Supplementary Figure 2.2 Encapsulation efficiency of DfAd-GFP.
The encapsulation efficiency of DfAd-GFP was measured at 96% by manually counting cryo-EM micrographs.

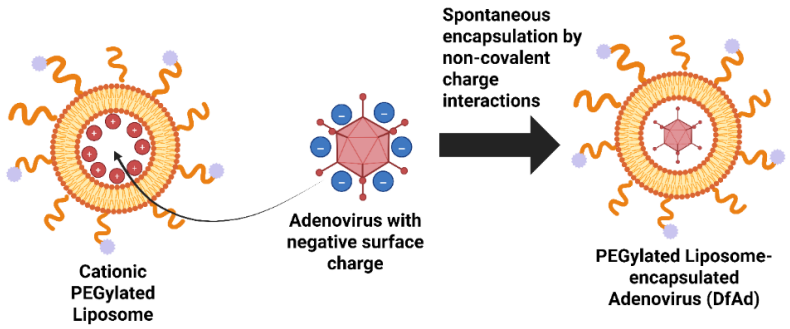

Supplementary Figure 2.3 Schematic of liposome encapsulation of adenovirus.
The spontaneous encapsulation of adenovirus by PEGylated liposomes hypothetically occurs due to favorable charge interactions between the negatively-charged hexon proteins of the adenovirus and the positively-charged liposome. Created in BioRender. Phung, A. (2025) https://BioRender.com/a1gghgc. Accessed 26 May 2025.

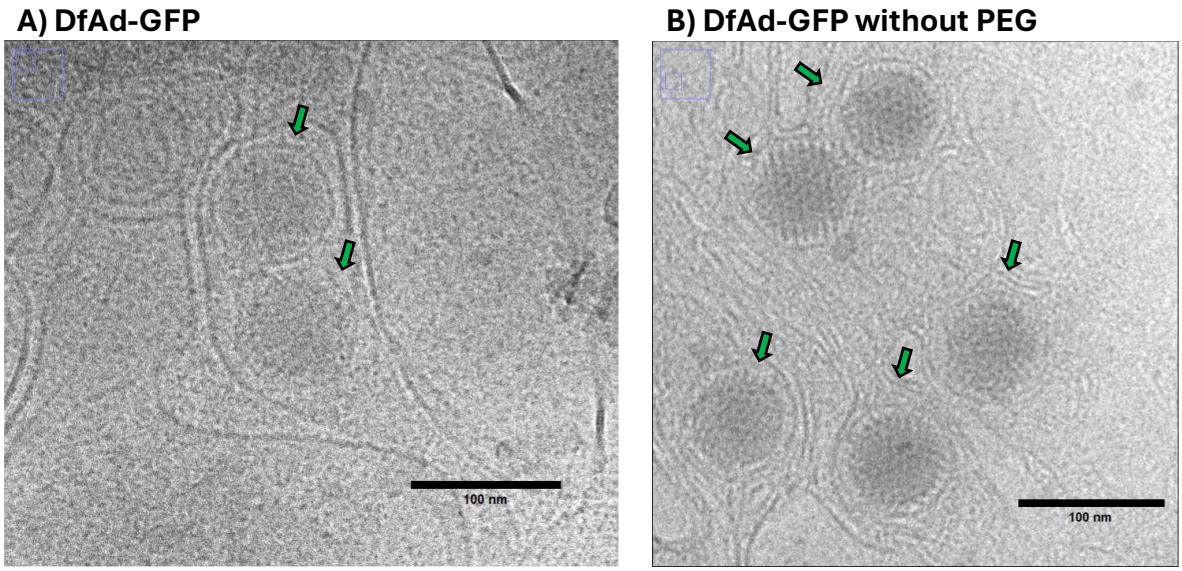

Supplementary Figure 2.4 Additional Characterization and Structural Analysis of DfAd.
(A) Cryo-TEM image of DfAd at 30,000× magnification plus a 50% digital zoom. Green arrows point to liposome-encapsulated Ad-GFP. This image appears to show two separate liposome-encapsulated Ad-GFP that are encapsulated together in a liposome. (B) Cryo-TEM image of DfAd-GFP without PEG at 30,000× magnification plus a 50% digital zoom. Green arrows point to liposome-encapsulated Ad-GFP. This image demonstrates tightly-enveloped DfAd without PPEG in a less bunched up group. In all figures, the scale bar for Cryo-TEM images is 100 nm.

2.9 References

1. Yan, Y.; Xu, H.; Wang, J.; Wu, X.; Wen, W.; Liang, Y.; Wang, L.; Liu, F.; Du, X. Inhibition of breast cancer cells by targeting E2F-1 gene and expressing IL15 oncolytic adenovirus. Bioscience Reports 2019, 39, BSR20190384, doi:10.1042/bsr20190384.

2. Carter, M.E.; Koch, A.; Lauer, U.M.; Hartkopf, A.D. Clinical Trials of Oncolytic Viruses in Breast Cancer. Frontiers in Oncology 2021, 11, doi:10.3389/fonc.2021.803050.

3. Ang, L.; Guo, L.; Wang, J.; Huang, J.; Lou, X.; Zhao, M. Oncolytic virotherapy armed with an engineered interfering lncRNA exhibits antitumor activity by blocking the epithelial mesenchymal transition in triple-negative breast cancer. Cancer Letters 2020, 479, 42-53, doi:10.1016/j.canlet.2020.03.012.

4. Ishikawa, W.; Kikuchi, S.; Ogawa, T.; Tabuchi, M.; Tazawa, H.; Kuroda, S.; Noma, K.; Nishizaki, M.; Kagawa, S.; Urata, Y.; Fujiwara, T. Boosting Replication and Penetration of Oncolytic Adenovirus by Paclitaxel Eradicate Peritoneal Metastasis of Gastric Cancer. Molecular Therapy - Oncolytics 2020, 18, 262-271, doi:10.1016/j.omto.2020.06.021.

5. Quixabeira, D.C.A.; Jirovec, E.; Pakola, S.; Havunen, R.; Basnet, S.; Santos, J.M.; Kudling, T.V.; Clubb, J.H.A.; Haybout, L.; Arias, V.; Grönberg-Vähä-Koskela, S.; Cervera-Carrascon, V.; Pasanen, A.; Anttila, M.; Tapper, J.; Kanerva, A.; Hemminki, A. Improving the cytotoxic response of tumor-infiltrating lymphocytes towards advanced stage ovarian cancer with an oncolytic adenovirus expressing a human vIL-2 cytokine. Cancer Gene Therapy 2023, 30, 1543-1553, doi:10.1038/s41417-023-00658-3.

6. Nassiri, F.; Patil, V.; Yefet, L.S.; Singh, O.; Liu, J.; Dang, R.M.A.; Yamaguchi, T.N.; Daras, M.; Cloughesy, T.F.; Colman, H.; Kumthekar, P.U.; Chen, C.C.; Aiken, R.; Groves, M.D.; Ong, S.S.; Ramakrishna, R.; Vogelbaum, M.A.; Khagi, S.; Kaley, T.; Melear, J.M.; Peereboom, D.M.; Rodriguez, A.; Yankelevich, M.; Nair, S.G.; Puduvalli, V.K.; Aldape, K.; Gao, A.; López-Janeiro, A.; de Andrea, C.E.; Alonso, M.M.; Boutros, P.; Robbins, J.; Mason, W.P.; Sonabend, A.M.; Stupp, R.; Fueyo, J.; Gomez-Manzano, C.; Lang, F.F.; Zadeh, G. Oncolytic DNX-2401 virotherapy plus pembrolizumab in recurrent glioblastoma: a phase 1/2 trial. Nature Medicine 2023, 29, 1370-1378, doi:10.1038/s41591-023-02347-y.

7. Xie, D.; Tian, Y.; Hu, D.; Wang, Y.; Yang, Y.; Zhou, B.; Zhang, R.; Ren, Z.; Liu, M.; Xu, J.; Dong, C.; Zhao, B.; Yang, L. Oncolytic adenoviruses expressing checkpoint inhibitors for cancer therapy. Signal Transduction and Targeted Therapy 2023, 8, 436, doi:10.1038/s41392-023-01683-2.

8. Quixabeira, D.C.A.; Zafar, S.; Santos, J.M.; Cervera-Carrascon, V.; Havunen, R.; Kudling, T.V.; Basnet, S.; Anttila, M.; Kanerva, A.; Hemminki, A. Oncolytic Adenovirus Coding for a Variant Interleukin 2 (vIL-2) Cytokine Re-Programs the Tumor Microenvironment and Confers Enhanced Tumor Control. Front Immunol 2021, 12, 674400, doi:10.3389/fimmu.2021.674400.

9. Yi, L.; Ning, Z.; Xu, L.; Shen, Y.; Zhu, X.; Yu, W.; Xie, J.; Meng, Z. The combination treatment of oncolytic adenovirus H101 with nivolumab for refractory advanced hepatocellular carcinoma: an open-label, single-arm, pilot study. ESMO Open 2024, 9, 102239, doi:10.1016/j.esmoop.2024.102239.

10. Atasheva, S.; Shayakhmetov, D.M. Oncolytic Viruses for Systemic Administration: Engineering a Whole Different Animal. Mol Ther 2021, 29, 904-907, doi:10.1016/j.ymthe.2021.02.001.

11. Andtbacka, R.H.; Ross, M.; Puzanov, I.; Milhem, M.; Collichio, F.; Delman, K.A.; Amatruda, T.; Zager, J.S.; Cranmer, L.; Hsueh, E.; Chen, L.; Shilkrut, M.; Kaufman, H.L. Patterns of Clinical Response with Talimogene Laherparepvec (T-VEC) in Patients with Melanoma Treated in the OPTiM Phase III Clinical Trial. Ann Surg Oncol 2016, 23, 4169-4177, doi:10.1245/s10434-016-5286-0.

12. Gómez, A.; Sardón, D.; Cejalvo, T.; Vázquez, F.; García-Castro, J.; Perisé-Barrios, A.J. Biodistribution Analysis of Oncolytic Adenoviruses in Canine Patient Necropsy Samples Treated with Cellular Virotherapy. Mol Ther Oncolytics 2020, 18, 525-534, doi:10.1016/j.omto.2020.08.006.

13. Zeng, M.; Zhang, W.; Li, Y.; Yu, L. Harnessing adenovirus in cancer immunotherapy: evoking cellular immunity and targeting delivery in cell-specific manner. Biomark Res 2024, 12, 36, doi:10.1186/s40364-024-00581-1.

14. Khare, R.; Hillestad, M.L.; Xu, Z.; Byrnes, A.P.; Barry, M.A. Circulating antibodies and macrophages as modulators of adenovirus pharmacology. J Virol 2013, 87, 3678-3686, doi:10.1128/jvi.01392-12.

15. Hemminki, O.; Dos Santos, J.M.; Hemminki, A. Oncolytic viruses for cancer immunotherapy. J Hematol Oncol 2020, 13, 84, doi:10.1186/s13045-020-00922-1.

16. Jirovec, E.; Quixabeira, D.C.A.; Clubb, J.H.A.; Pakola, S.A.; Kudling, T.; Arias, V.; Haybout, L.; Jalkanen, K.; Alanko, T.; Monberg, T.; Khammari, A.; Dreno, B; Svane, I.M.; Block, M.S.; Adamo, D.A.; Mäenpää, J.; Kistler, C.; Sorsa, S.; Hemminki, O.; Kanerva, A.; Santos, J.M.; Cervera-Carrascon, V.; Hemminki, A. Single intravenous administration of oncolytic adenovirus TILT-123 results in systemic tumor transduction and immune response in patients with advanced solid tumors. J Exp Clin Cancer Res 2024, 43, 297, doi:10.1186/s13046-024-03219-0.

17. Heo, J.; Liang, J.D.; Kim, C.W.; Woo, H.Y.; Shih, I.L.; Su, T.H.; Lin, Z.Z.; Yoo, S.Y.; Chang, S.; Urata, Y.; Chen, P.-J. Safety and dose escalation of the targeted oncolytic adenovirus OBP-301 for refractory advanced liver cancer: Phase I clinical trial. Mol Ther 2023, 31, 2077-2088, doi:10.1016/j.ymthe.2023.04.006.

18. Garcia-Carbonero, R.; Bazan-Peregrino, M.; Gil-Martín, M.; Álvarez, R.; Macarulla, T.; Riesco-Martinez, M.C.; Verdaguer, H.; Guillén-Ponce, C.; Farrera-Sal, M.; Moreno, R.; Mato-

Berciano, A.; Maliandi, M.V.; Torres-Manjon, S.; Costa, M.; Del Pozo, N.; Martínez de Villarreal, J.; Real, F.X.; Vidal, N.; Capella, G.; Alemany, R.; Blasi, E.; Blasco, C.; Cascalló, M.; Salazar, R. Phase I, multicenter, open-label study of intravenous VCN-01 oncolytic adenovirus with or without nab-paclitaxel plus gemcitabine in patients with advanced solid tumors. J Immunother Cancer 2022, 10, doi:10.1136/jitc-2021-003255.

19. Santos, J.; Heiniö, C.; Quixabeira, D.; Zafar, S.; Clubb, J.; Pakola, S.; Cervera-Carrascon, V.; Havunen, R.; Kanerva, A.; Hemminki, A. Systemic Delivery of Oncolytic Adenovirus to Tumors Using Tumor-Infiltrating Lymphocytes as Carriers. Cells 2021, 10, doi:10.3390/cells10050978.

20. Thambi, T.; Hong, J.; Yoon, A.R.; Yun, C.-O. Challenges and progress toward tumor-targeted therapy by systemic delivery of polymer-complexed oncolytic adenoviruses. Cancer Gene Therapy 2022, 29, 1321-1331, doi:10.1038/s41417-022-00469-y.

21. Zhao, Y.; Liu, Z.; Li, L.; Wu, J.; Zhang, H.; Lei, T.; Xu, B. Oncolytic Adenovirus: Prospects for Cancer Immunotherapy. Front Microbiol 2021, 12, 707290, doi:10.3389/fmicb.2021.707290.

22. Mendez, N.; Herrera, V.; Zhang, L.; Hedjran, F.; Feuer, R.; Blair, S.L.; Trogler, W.C.; Reid, T.R.; Kummel, A.C. Encapsulation of adenovirus serotype 5 in anionic lecithin liposomes using a bead-based immunoprecipitation technique enhances transfection efficiency. Biomaterials 2014, 35, 9554-9561, doi:10.1016/j.biomaterials.2014.08.010.

23. Huang, C.-H.; Dong, T.; Phung, A.T.; Shah, J.R.; Larson, C.; Sanchez, A.B.; Blair, S.L.; Oronsky, B.; Trogler, W.C.; Reid, T.; Kummel, A.C. Full Remission of CAR-Deficient Tumors by DOTAP-Folate Liposome Encapsulation of Adenovirus. ACS Biomaterials Science & Engineering 2022, 8, 5199-5209, doi:10.1021/acsbiomaterials.2c00966.

24. Shah, J.R.; Dong, T.; Phung, A.T.; Reid, T.; Larson, C.; Sanchez, A.B.; Oronsky, B.; Blair, S.L.; Aisagbonhi, O.; Trogler, W.C.; Kummel, A.C. Development of Adenovirus Containing Liposomes Produced by Extrusion vs. Homogenization: A Comparison for Scale-Up Purposes. Bioengineering 2022, 9, 620, doi:10.3390/bioengineering9110620.

25. Dong, T.; Shah, J.R.; Phung, A.T.; Larson, C.; Sanchez, A.B.; Aisagbonhi, O.; Blair, S.L.; Oronsky, B.; Trogler, W.C.; Reid, T.; Kummel, A.C. A Local and Abscopal Effect Observed with Liposomal Encapsulation of Intratumorally Injected Oncolytic Adenoviral Therapy. Cancers 2023, 15, 3157, doi:10.3390/cancers15123157.

26. Phung, A.T.; Shah, J.R.; Dong, T.; Reid, T.; Larson, C.; Sanchez, A.B.; Oronsky, B.; Trogler, W.C.; Kummel, A.C.; Aisagbonhi, O.; Blair, S.L. CAR expression in invasive breast carcinoma and its effect on adenovirus transduction efficiency. Breast Cancer Research 2024, 26, 131, doi:10.1186/s13058-024-01880-z.

27. Yotnda, P.; Chen, D.H.; Chiu, W.; Piedra, P.A.; Davis, A.; Templeton, N.S.; Brenner, M.K. Bilamellar cationic liposomes protect adenovectors from preexisting humoral immune

responses. Mol Ther 2002, 5, 233-241, doi:10.1006/mthe.2002.0545.

28. Steel, J.C.; Cavanagh, H.M.; Burton, M.A.; Dingwall, D.J.; Kalle, W.H. Modification of liposomal concentration in liposome/adenoviral complexes allows significant protection of adenoviral vectors from neutralising antibody, in vitro. J Virol Methods 2005, 126, 31-36, doi:10.1016/j.jviromet.2005.01.017.

29. Liu, S.-H.; Smyth-Templeton, N.; Davis, A.R.; Davis, E.A.; Ballian, N.; Li, M.; Liu, H.; Fisher, W.; Brunicardi, F.C. Multiple treatment cycles of liposome-encapsulated adenoviral RIP-TK gene therapy effectively ablate human pancreatic cancer cells in SCID mice. Surgery 2011, 149, 484-495, doi:10.1016/j.surg.2010.11.014.

30. Ganesan, L.P.; Mohanty, S.; Kim, J.; Clark, K.R.; Robinson, J.M.; Anderson, C.L. Rapid and efficient clearance of blood-borne virus by liver sinusoidal endothelium. PLoS Pathog 2011, 7, e1002281, doi:10.1371/journal.ppat.1002281.

31. Welsher, K.; Sherlock, S.P.; Dai, H. Deep-tissue anatomical imaging of mice using carbon nanotube fluorophores in the second near-infrared window. Proc Natl Acad Sci U S A 2011, 108, 8943-8948, doi:10.1073/pnas.1014501108.

32. Naumenko, V.A.; Vishnevskiy, D.A.; Stepanenko, A.A.; Sosnovtseva, A.O.; Chernysheva, A.A.; Abakumova, T.O.; Valikhov, M.P.; Lipatova, A.V.; Abakumov, M.A.; Chekhonin, V.P. In Vivo Tracking for Oncolytic Adenovirus Interactions with Liver Cells. Biomedicines 2022, 10, doi:10.3390/biomedicines10071697.

33. Shayakhmetov, D.M.; Li, Z.Y.; Ni, S.; Lieber, A. Analysis of adenovirus sequestration in the liver, transduction of hepatic cells, and innate toxicity after injection of fiber-modified vectors. J Virol 2004, 78, 5368-5381, doi:10.1128/jvi.78.10.5368-5381.2004.

34. Tao, N.; Gao, G.P.; Parr, M.; Johnston, J.; Baradet, T.; Wilson, J.M.; Barsoum, J.; Fawell, S.E. Sequestration of adenoviral vector by Kupffer cells leads to a nonlinear dose response of transduction in liver. Mol Ther 2001, 3, 28-35, doi:10.1006/mthe.2000.0227.

35. Yoon, A.R.; Hong, J.; Kim, M.; Yun, C.-O. Hepatocellular carcinoma-targeting oncolytic adenovirus overcomes hypoxic tumor microenvironment and effectively disperses through both central and peripheral tumor regions. Scientific Reports 2018, 8, 2233, doi:10.1038/s41598-018-20268-6.

36. Zhang, Z.; Krimmel, J.; Hu, Z.; Seth, P. Systemic delivery of a novel liver-detargeted oncolytic adenovirus causes reduced liver toxicity but maintains the antitumor response in a breast cancer bone metastasis model. Hum Gene Ther 2011, 22, 1137-1142, doi:10.1089/hum.2011.003.

37. Zhao, Y.; Le, T.M.D.; Hong, J.; Jiao, A.; Yoon, A.R.; Yun, C.-O. Smart Accumulating Dual-Targeting Lipid Envelopes Equipping Oncolytic Adenovirus for Enhancing Cancer Gene Therapeutic Efficacy. ACS Nano 2024, 18, 27869-27890, doi:10.1021/acsnano.4c02165.

38. Shah, J.R.; Dong, T.; Phung, A.T.; Khan, S.; Aisagbonhi, O.; Blair, S.L.; Bouvet, M.; Trogler, W.C.; Kummel, A.C. Liposomal oncolytic adenovirus as a neoadjuvant therapy for triple-negative breast cancer. Scientific Reports 2025, 15, 16737, doi:10.1038/s41598-025-00211-2.

39. Azumah, J.; Smistad, G.; Hiorth, M. Preparation of stable polymer-liposome complexes by a novel approach employing a one-pot method. Colloids and Surfaces A: Physicochemical and Engineering Aspects 2022, 653, 129924, doi:https://doi.org/10.1016/j.colsurfa.2022.129924.

40. Suk, J.S.; Xu, Q.; Kim, N.; Hanes, J.; Ensign, L.M. PEGylation as a strategy for improving nanoparticle-based drug and gene delivery. Adv Drug Deliv Rev 2016, 99, 28-51, doi:10.1016/j.addr.2015.09.012.

41. Santhanakrishnan, K.R.; Koilpillai, J.; Narayanasamy, D. PEGylation in Pharmaceutical Development: Current Status and Emerging Trends in Macromolecular and Immunotherapeutic Drugs. Cureus 2024, 16, e66669, doi:10.7759/cureus.66669.

42. Nag, O.K.; Awasthi, V. Surface engineering of liposomes for stealth behavior. Pharmaceutics 2013, 5, 542-569, doi:10.3390/pharmaceutics5040542.

43. Kowalska, M.; Broniatowski, M.; Mach, M.; Płachta, Ł.; Wydro, P. The effect of the polyethylene glycol chain length of a lipopolymer (DSPE-PEGn) on the properties of DPPC monolayers and bilayers. Journal of Molecular Liquids 2021, 335, 116529, doi:https://doi.org/10.1016/j.molliq.2021.116529.

44. El-Baz, N.; Nunn, B.M.; Bates, P.J.; O'Toole, M.G. The Impact of PEGylation on Cellular Uptake and In Vivo Biodistribution of Gold Nanoparticle MRI Contrast Agents. Bioengineering 2022, 9, doi:10.3390/bioengineering9120766.

45. Zhang, H.; Barz, M. Investigating the stability of RNA-lipid nanoparticles in biological fluids: Unveiling its crucial role for understanding LNP performance. Journal of Controlled Release 2025, 381, 113559, doi:https://doi.org/10.1016/j.jconrel.2025.02.055.

46. Marín, D.; Alemán, A.; Sánchez-Faure, A.; Montero, P.; Gómez-Guillén, M.C. Freeze-dried phosphatidylcholine liposomes encapsulating various antioxidant extracts from natural waste as functional ingredients in surimi gels. Food Chemistry 2018, 245, 525-535, doi:https://doi.org/10.1016/j.foodchem.2017.10.141.

47. Xia, Y.; Sun, J.; Liang, D. Aggregation, Fusion, and Leakage of Liposomes Induced by Peptides. Langmuir 2014, 30, 7334-7342, doi:10.1021/la501618f.

48. Xu, X.; Tian, F.; Pan, Y.; Zhang, T.; Deng, L.; Jiang, H.; Han, J.; Liu, J.; Zhao, Y.; Liu, W. Emerging mechanistic insights into liposomal stability: Full process management from production and storage to food application. Chemical Engineering Journal 2025, 505, 159552, doi:https://doi.org/10.1016/j.cej.2025.159552.

49. Yu, J.Y.; Chuesiang, P.; Shin, G.H.; Park, H.J. Post-Processing Techniques for the Improvement of Liposome Stability. Pharmaceutics 2021, 13, doi:10.3390/pharmaceutics13071023.